AD-A107 637 GEO-ATMOSPHERICS CORP LINCOLN MA F/G 20/6

MODELS OF WEATHER ENVIRONMENTS ADVERSE TO ELECTRO-OPTICAL SYSTE--ETC(U)

SEP 81 W D MOUNT, B R FOW DAAD07-80-C-0047

UNCLASSIFIED ERADCOM/ASL-CR-81-0047-1 NL

1 OF 2

AD A

107637

AD A107637

CR-81-0047-1

AD

Reports Control Symbol
OSD - 1366

LEVEL II

(12)

MODELS OF WEATHER ENVIRONMENTS ADVERSE TO ELECTRO-OPTICAL SYSTEMS

SEPTEMBER 1981

Prepared by

Wayne D. Mount
B. Richard Fow

Geo-Atmospherics Corporation
Box 177
Lincoln, Massachusetts 01773

Under Contract DAAD07-80-C-0047
Contract Monitor: Ronald M. Cionco

Approved for public release; distribution unlimited.

US Army Electronics Research and Development Command
Atmospheric Sciences Laboratory
White Sands Missile Range, NM 88002

NOTICES

Disclaimers

Disposition

CR-81-0047-1
DAAD07-80-C-0047

ERRATA SHEET

The following items are reproduced on this errata sheet to improve clarity: (1) Figure 20, from page 74; (2) Table 7, from page 81; (3) Table 8, from page 82; and (4) Table 9, from page 83.

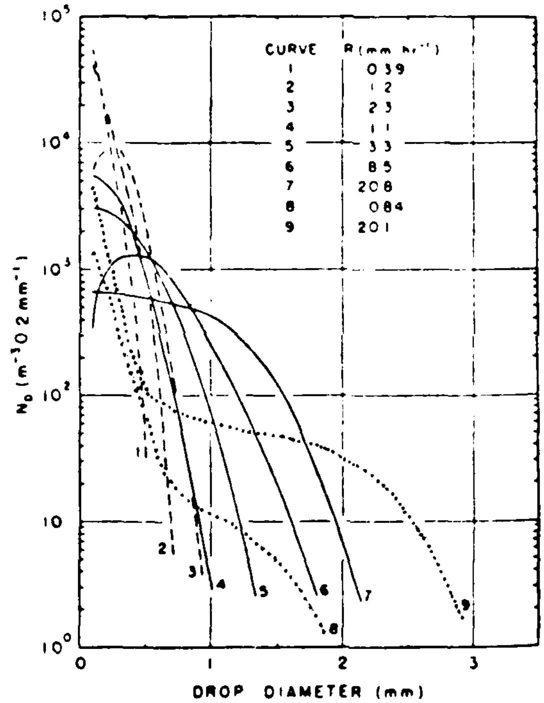

Fig. 20 Variety of Raindrop Size Distributions

TABLE 7. MODERATE RAIN (6 MM/HR) FOR SUMMER MID-LATITUDES

RAIN MODEL ATMOSPHERE - MODERATE RAIN - 6 MM/HR 45 N MODEL - MID-LATITUDE

HEIGHT (KM)	PRESSURE (MB)	TEMPERATURE (DEG K)	RELATIVE HUMIDITY	CLOUD CONTENT (GM/CU M)	RAIN RATE (MM/HR)
0.000	1013.00	287.20	1.000	0.0000	6.000
.250	983.00	286.20	1.000	.2000	5.500
.500	954.00	285.10	1.000	.2800	4.400
.750	926.00	284.00	1.000	.3200	3.500
1.000	899.00	282.70	1.000	.3300	3.000
1.250	872.00	281.20	1.000	.3400	2.400
1.500	846.00	280.00	1.000	.3500	1.900
1.750	820.00	278.50	1.000	.3500	1.500
2.000	795.00	277.30	1.000	.3500	1.100
2.500	747.00	274.40	1.000	.3500	.600
3.000	701.00	271.20	1.000	.3500	.200
3.500	658.00	268.50	1.000	.3100	-0.000
4.000	616.00	265.00	1.000	.2500	-0.000
4.500	577.00	261.00	1.000	.1800	-0.000
5.000	540.00	258.00	1.000	.1300	-0.000
5.500	505.00	254.50	1.000	.0900	-0.000
6.000	472.00	251.50	1.000	.0500	-0.000
6.500	440.00	246.20	1.000	.0300	-0.000
7.000	410.00	242.20	1.000	.0100	-0.000
7.500	382.00	238.00	1.000	-0.0000	-0.000
8.000	356.00	234.50	1.000	-0.0000	-0.000
8.500	330.00	229.00	1.000	-0.0000	-0.000
9.000	307.00	225.00	.980	-0.0000	-0.000
9.500	285.00	220.00	.950	-0.0000	-0.000
10.000	264.00	223.20	.850	-0.0000	-0.000
11.000	226.00	216.70	.400	-0.0000	-0.000
12.000	193.00	216.70	.160	-0.0000	-0.000
13.000	165.00	216.70	.060	-0.0000	-0.000
14.000	141.00	216.70	.041	-0.0000	-0.000
15.000	120.00	216.70	.031	-0.0000	-0.000
16.000	103.00	216.70	.023	-0.0000	-0.000
17.000	87.98	216.70	.019	-0.0000	-0.000
18.000	75.00	216.70	.016	-0.0000	-0.000
19.000	64.10	216.70	.014	-0.0000	-0.000
20.000	54.70	216.70	.012	-0.0000	-0.000
22.000	40.00	218.70	.007	-0.0000	-0.000
24.000	29.30	220.70	.004	-0.0000	-0.000
26.000	21.50	222.70	.002	-0.0000	-0.000
28.000	15.90	224.70	.001	-0.0000	-0.000
30.000	11.70	226.70	-0.000	-0.0000	-0.000
35.000	5.60	237.00	-0.000	-0.0000	-0.000
40.000	2.80	251.00	-0.000	-0.0000	-0.000
45.000	1.40	265.00	-0.000	-0.0000	-0.000
50.000	.80	270.70	-0.000	-0.0000	-0.000

TABLE 8 HEAVY RAIN (15 MM/HR) FOR MID-LATITUDES

RAIN MODEL ATMOSPHERE - HEAVY RAIN - 15 MM/HR 45 N MODEL - MID-LATITUDE

HEIGHT (KM)	PRESSURE (MB)	TEMPERATURE (DEG K)	RELATIVE HUMIDITY	CLOUD CONTENT (GM/CU M)	RAIN RATE (MM/HR)
0.000	1013.00	287.20	1.000	0.0000	15.000
.250	983.00	286.20	1.000	.3000	14.600
.500	954.00	285.10	1.000	.4000	14.300
.750	926.00	284.00	1.000	.4300	13.900
1.000	899.00	282.70	1.000	.4500	13.500
1.250	872.00	281.20	1.000	.4500	13.200
1.500	846.00	280.00	1.000	.4500	12.900
1.750	820.00	278.50	1.000	.4500	12.400
2.000	795.00	277.30	1.000	.4500	12.100
2.500	747.00	274.40	1.000	.4500	11.600
3.000	701.00	271.20	1.000	.4500	3.100
3.500	658.00	268.50	1.000	.4500	.010
4.000	616.00	265.00	1.000	.4500	-0.000
4.500	577.00	261.00	1.000	.3000	-0.000
5.000	540.00	258.00	1.000	.1700	-0.000
5.500	505.00	254.50	1.000	.1000	-0.000
6.000	472.00	251.50	1.000	.0500	-0.000
6.500	440.00	246.20	1.000	.0300	-0.000
7.000	410.00	242.20	1.000	.0100	-0.000
7.500	382.00	230.00	1.000	-0.0000	-0.000
8.000	356.00	234.50	1.000	-0.0000	-0.000
8.500	330.00	229.00	1.000	-0.0000	-0.000
9.000	307.00	225.00	.980	-0.0000	-0.000
9.500	205.00	220.00	.950	-0.0000	-0.000
10.000	264.00	223.20	.850	-0.0000	-0.000
11.000	226.00	216.70	.600	-0.0000	-0.000
12.000	193.00	216.70	.160	-0.0000	-0.000
13.000	165.00	216.70	.060	-0.0000	-0.000
14.000	141.00	216.70	.041	-0.0000	-0.000
15.000	120.00	216.70	.031	-0.0000	-0.000
16.000	103.00	216.70	.023	-0.0000	-0.000
17.000	87.90	216.70	.019	-0.0000	-0.000
18.000	75.00	216.70	.016	-0.0000	-0.000
19.000	64.10	216.70	.014	-0.0000	-0.000
20.000	54.70	216.70	.012	-0.0000	-0.000
22.000	40.00	218.70	.007	-0.0000	-0.000
24.000	29.30	220.70	.004	-0.0000	-0.000
26.000	21.50	222.70	.002	-0.0000	-0.000
28.000	15.90	224.70	.001	-0.0000	-0.000
30.000	11.70	226.70	-0.000	-0.0000	-0.000
35.000	5.60	237.00	-0.000	-0.0000	-0.000
40.000	2.80	251.00	-0.000	-0.0000	-0.000
45.000	1.40	265.00	-0.000	-0.0000	-0.000
50.000	.80	270.70	-0.000	-0.0000	-0.000

TABLE 9 HEAVY RAIN (15 MM/HR) FOR TROPICAL LATITUDES

TROPICAL - 15 N HEAVY RAIN OF 15 MM/HR

HEIGHT (KM)	PRESSURE (MB)	TEMPERATURE (DEG K)	RELATIVE HUMIDITY	CLOUD CONTENT (GM/CU M)	RAIN RATE (MM/HR)
0.000	1013.00	298.00	.900	-0.0000	15.000
.250	985.00	297.20	1.000	.2000	14.500
.500	957.00	296.00	1.000	.3500	14.000
.750	930.00	295.00	1.000	.4000	13.500
1.000	904.00	293.00	1.000	.4500	13.000
1.250	878.00	293.10	1.000	.4500	12.600
1.500	853.00	292.60	1.000	.4500	12.200
1.750	828.00	291.40	1.000	.4500	11.900
2.000	804.00	269.50	1.000	.4500	11.600
2.500	758.00	287.10	1.000	.4500	11.000
3.000	714.00	285.10	1.000	.4500	10.500
3.500	672.00	282.00	1.000	.4500	10.200
4.000	632.00	280.60	1.000	.4500	9.900
4.500	594.00	278.00	1.000	.4500	9.700
5.000	558.00	275.40	1.000	.4500	9.500
5.500	524.00	273.00	1.000	.4500	5.500
6.000	491.00	270.20	1.000	.4500	.800
6.500	460.00	267.20	1.000	.4400	.200
7.000	431.00	264.30	1.000	.3600	.100
7.500	403.00	261.20	1.000	.3000	-0.000
8.000	376.00	257.80	1.000	.2500	-0.000
8.500	351.00	254.40	1.000	.1900	-0.000
9.000	328.00	251.00	1.000	.1400	-0.000
9.500	305.00	248.00	1.000	.0800	-0.000
10.000	284.00	242.90	1.000	.0300	-0.000
11.000	247.00	234.80	1.000	.0200	-0.000
12.000	211.00	235.60	1.000	.0100	-0.000
13.000	181.00	216.20	1.000	-0.0000	-0.000
14.000	154.00	206.30	1.000	-0.0000	-0.000
15.000	131.00	196.50	1.000	-0.0000	-0.000
16.000	110.00	192.60	.600	-0.0000	-0.000
17.000	92.30	194.80	.350	-0.0000	-0.000
18.000	77.60	198.80	.120	-0.0000	-0.000
19.000	65.50	202.80	.055	-0.0000	-0.000
20.000	55.50	206.70	.025	-0.0000	-0.000
22.000	40.10	214.60	.008	-0.0000	-0.000
24.000	29.30	219.20	.002	-0.0000	-0.000
26.000	21.50	223.60	.001	-0.0000	-0.000
28.000	16.90	227.90	-0.000	-0.0000	-0.000
30.000	11.80	232.40	-0.000	-0.0000	-0.000
35.000	5.84	245.00	-0.000	-0.0000	-0.000
40.000	2.99	258.50	-0.000	-0.0000	-0.000
45.000	1.58	269.00	-0.000	-0.0000	-0.000
50.000	.86	273.00	-0.000	-0.0000	-0.000

SECURITY CLASSIFICATION OF THIS PAGE (When Data Entered)

REPORT DOCUMENTATION PAGE		READ INSTRUCTIONS BEFORE COMPLETING FORM
1. REPORT NUMBER ASL-CR-81-0047-1	2. GOVT ACCESSION NO. AD-107 637	3. RECIPIENT'S CATALOG NUMBER
4. TITLE (and Subtitle) MODELS OF WEATHER ENVIRONMENTS ADVERSE TO ELECTRO-OPTICAL SYSTEMS		5. TYPE OF REPORT & PERIOD COVERED Contractor Report 6. PERFORMING ORG. REPORT NUMBER
7. AUTHOR(s) Wayne D. Mount and B. Richard Fow		8. CONTRACT OR GRANT NUMBER(s) DAAD07-80-C-0047
9. PERFORMING ORGANIZATION NAME AND ADDRESS Geo-Atmospherics Corporation Box 177 Lincoln, MA 01773		10. PROGRAM ELEMENT, PROJECT, TASK AREA & WORK UNIT NUMBERS DA Task 1L161102B53A
11. CONTROLLING OFFICE NAME AND ADDRESS US Army Electronics Research and Development Command Adelphi, MD 20783		12. REPORT DATE September 1981 13. NUMBER OF PAGES 107
14. MONITORING AGENCY NAME & ADDRESS(if different from Controlling Office) US Army Atmospheric Sciences Laboratory White Sands Missile Range, NM 88002		15. SECURITY CLASS. (of this report) UNCLASSIFIED 15a. DECLASSIFICATION/DOWNGRADING SCHEDULE

16. DISTRIBUTION STATEMENT (of this Report)

Approved for public release; distribution unlimited

17. DISTRIBUTION STATEMENT (of the abstract entered in Block 20, if different from Report)

18. SUPPLEMENTARY NOTES

Contract Monitor: Ronald M. Cionco

19. KEY WORDS (Continue on reverse side if necessary and identify by block number)

Adverse weather	Fog	Particle size distribution
Electro-optical systems	Clouds	Meteorological data
Dynamic models	Rain	Liquid water content
Haze	Scattering	Visibility

20. ABSTRACT (Continue on reverse side if necessary and identify by block number)

Weather models are developed to depict hour by hour variations of scattering media--the atmosphere--important to Army electro-optical system performance. Dynamic models are presented for specifying particle size distributions in horizontal and vertical directions for haze, fog, cloud, and rain conditions given only routinely available meteorological data. Case studies show that these models perform well individually and when used together. This effort should be viewed as the first step in developing dynamic models that are

DD FORM 1 JAN 73 1473 EDITION OF 1 NOV 65 IS OBSOLETE

SECURITY CLASSIFICATION OF THIS PAGE (When Data Entered)

20. ABSTRACT (cont)

responsive to observed and forecast weather changes. The models needed to be applied, tested, modified, and improved.

Accession For

A

TABLE OF CONTENTS

2 (cont.)

ILLUSTRATIONS

ILLUSTRATIONS (continued #2)

TABLES

I INTRODUCTION

1.1 GENERAL

1.1.1 <u>Contract/Scope</u>

This work was accomplished under Contract Number DAAD07-80-C-[illegible]47 with the U.S. Army White Sands Missile Range. The contract became effective on 7 February 1980 and constituted less than one half man year of technical effort. The Contracting Officer's Technical Representative is:

Mr. Ronald Cionco
Atmospheric Sciences Laboratory
Attn: DELAS-BE-C
White Sands Missile Range, NM 88002

1.1.2 Overview

Environmental conditions often dictate effectiveness of Army offensive and defensive weapon systems. Such things as terrain, vegetation, and weather determine in what direction, how far, and what degree of clarity a target can be acquired, isolated, and distinguished from its surroundings. For a particular season and theater of operation, weather offers the greatest day to day change that influences weapon system performance. Studies are being conducted to develop techniques to determine "seeability" or obscuration from natural as well as battlefield induced contaminates. Considerable attention is being directed towards electro-optical (EO) energy absorption due to gaseous molecules, scattering due to haze, smoke, fog, cloud, rain, snow or hail, and beam wandering due to small scale turbulence and temperature fluctuations. Obscuration due to scattering, however, depends greatly upon the energy wavelength of the viewing sensor relative to type, number and size distribution of atmospheric litho- and hydrometeors.

The scattering process itself behaves nonlinearly and, by necessity, obscuration models must consider such meteorological microphysical features as number concentration and size distribution of particles. It is unreasonable to expect observations of these microphysical features within a battlefield environment. Thus it becomes necessary to work within the scope of routinely available weather information to infer the microfea-

tures and to define the actual scattering medium. Geo-Atmospherics Corporation has developed weather models to depict hour by hour variations of scattering media important to Army weapon system performance.

Better instruments and experimental data gathering programs are necessary to establish reliable data bases of atmospheric microphysical features of liquid and solid particles associated with the wide range of possible global weather. These data must have the accuracy demanded for basic studies on their impact on design and operation of EO systems. To date, a number of static models have been developed to represent atmospheric particles for a particular type of environment. For example, aerosol models have been generated to represent "typical" conditions expected to be found in Continental or maritime regions or at different levels in the atmosphere. Some of these models are:

A. Rural Model -	which is to represent the natural midlatitude environment found in the country or in clean air urban regions found after a cold front passage.
B. Urban Model -	which is to represent the industrial aerosols found in cities and in rural regions experiencing air stagnation and subsequent air pollution build-up.
C. Maritime Model -	which is to represent the open ocean regions at least 300 km offshore with a moderate surface air wind speed.

D. Tropospheric Model - which is to normally represent the turbulent layer of the atmosphere between the top of the boundary layer (about 2 km) and the tropopause (9 to 18 km, depending upon season and, to a greater extent, latitude) as well as those special boundary layer cases when the surface air layer over land is calm and clean (meteorological range greater than 40 km).

E. High Level Models - which is to represent aerosol distributions within the stable stratosphere (from the tropopause to about 20 km) and the mesosphere (from the top of the stratosphere to about 80 km).

Similar types of static models have been developed for fog, cloud, and rain conditions. The atmosphere is, however, a fluid in motion that produces continuous rather than discrete spectrums.

What we have done here is to take the first step in developing dynamic models that relate particle type, concentration, size distribution, and their vertical variation to observed dynamics and thermodynamics of the atmosphere that exist at any instant in time. A ground rule established was that only routinely available standard surface and upper air observations and/or forecasts would be available for use in a real-world battlefield environment. As such, a number of simplifying assumptions had to be made, to use meso and synoptic scale data to depict microscale features. Not all gaps were closed and much remains to be done but significant advances

were made in dynamically modeling litho- and hydro-meters important to operational performance of Electro - Optical Systems.

1.2 MODELING EQUATIONS

1.2.1 General

There is no question that adverse weather is detrimental to electromagnetic energy propagation. Theoretical and application techniques have been developed to simulate atmospheric radiative transfer effects to derive obscuration expected for any sensor. What is required is a quantitative description of the scattering medium that is needed in order to be able to derive obscuration. The problem is how to map three dimensional distributions of microphysical scattering media given only routinely available surface and upper air meteorological information.

Before dicussing the techniques used to develop the dynamical models for fog, cloud, and rain conditions, it is worthwhile to consider the different characteristics associated with the two most popular analytical methods used to depict particle size distributions, namely the power law and the exponential (modified gamma) equations. The equations will be presented and discussed to show shapes and characteristics responsive to the wide variety of atmospheric particles. For the purposes of this study the particle sizes vary by six orders of magnitude. Each type of particle has a typical mode radius and range of values, as shown in Table I. Although size distributions vary within each category which must be considered, it is equally important to develop modeling schemes that account for the extreme variations among different meteorological events.

TABLE I Typical Atmospheric Particle Sizes

Particle Type	Mode Radius micrometers	Radius Range micrometers
Continental Aerosols	0.02	.002 - 20
Maritime Aerosols	0.2	.02 - 20
New Fog (1 hr)	4	1 - 40
Old (Evolved) Fog (2 hr)	10	1 - 80
Fair Weather Cumulus	3.5	1 - 10
Stratus/Stratocumulus	4	1 - 15
Altostratus	5	1 - 13
Nimbostratus	5	1 - 40
Cumulonimbus	6	1 - 100
Mist (0.05 mm/hr)	75	6 - 550
Drizzle (0.25 mm/hr)	150	6 - 750
Light Rain (1 mm/hr)	175	6 - 1250
Moderate Rain (4 mm/hr)	200	6 - 1750
Heavy Rain (16 mm/hr)	225	6 - 2250

1.2.2 Power Law Size Distribution

One of the most popular methods in use today to represent solid aerosols in the atmosphere was developed by Junge in 1958. From many of his aerosol measurement studies he found the concentration peaked at a radius of about 0.02 μm but remained linearly distributed between about 0.1 to 10 μm, when plotted on a log log scale. This linear range covers the most optically interesting phenomena in a hazy atmosphere. The smaller aerosols in this range provide a bluish tinge to thin haze, those around 0.3 μm are most important in determining what we call visibility in haze, and the larger aerosols, which are fewer in number, can provide beautiful red sunsets. Therefore, Junge's power law representation of aerosol size distribution and concentration is very appropriate in defining EO responses to haze and it is simple to derive from measured data and simple to use.

Junge's power - law size distribution function is:

$$n(r) = \frac{d\ N}{d\ \log\ r} = C\ r^{-v} \qquad (1)$$

where n(r) is the number of particles per unit interval of radius and per unit volume, C is the surface air particle concentration factor, r is the aerosol radius in μm, and the exponent v defines the slope of the distribution curve.

Often the nonlogarithmic form of equation (1) is desired. Since

$d \log r = 0.434\ d \ln r$ and $d \ln r = \frac{dr}{r}$

then equation (1) can be rewritten as:

$$n(r) = \frac{dN}{dr} = 0.434\, C\, r^{-(v+1)} \tag{2}$$

We will use this form of the power - law equation. Therefore the particle concentration (N) say for all particles equal to or greater than radius r, becomes the integral of equation (2) as

$$N = 0.434\, C \int_{r_1}^{\alpha} r^{-(v+1)}\, dr \tag{3}$$

The units for droplet or aerosol concentrations, n (r), are $cm^{-3}\ \mu m^{-1}$. Therefore the units for total particle concentrations above a given radius are cm^{-3}.

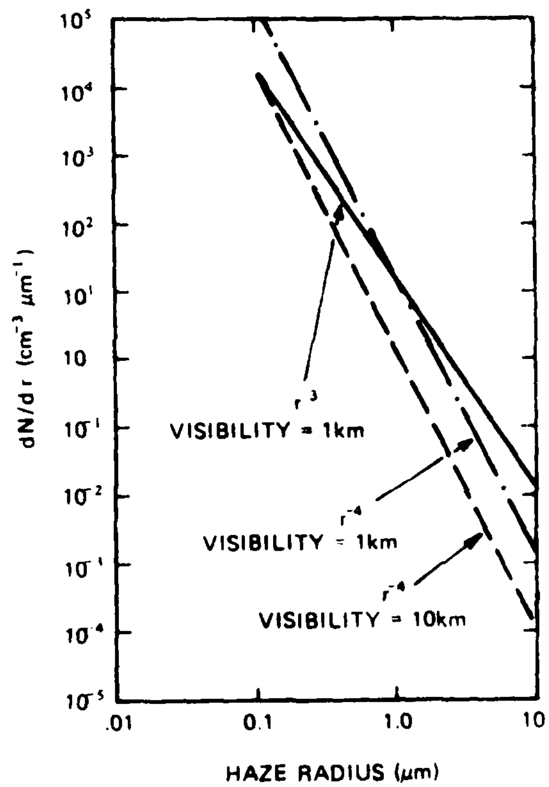

Fig. 1. Power Law Size Distributions.

Figure 1 shows how the power law size distribution given in Eq. (2) varies as a function of the exponent v and the factor C. Plotted in Fig. 1 is the aerosol concentration as a function of haze particle size radius. These plots are made for continental air near the earth's surface assuming two different slope factors v and two visibilities, which effect the concentration factor C. Later we will describe the rational and equations we developed to specify C and v according to changing meteorological features. For now, we want to demonstrate how the power law distribution changes with a fixed C and variable v and for a fixed v with variable C. Fig. 1 shows two visibilities, 1 and 10 km, which translates to concentration factors C of 30 and 3, respectively. The exponents shown correspond to v values of 3 and 2.

Notice in Fig. 1 for a constant concentration factor, visibility 1 km, as the exponent slope factor v decreases in value the aerosol size distribution curve becomes more shallow resulting in fewer numbers of smaller particles and larger concentrations of larger size particles. Typical values of v are 2 and 3 for fog and haze particles, respectively, and are shown plotted in Fig. 1 for 1 km visibility conditions. It is not unusual to have both haze and fog present during 1 km visibility conditions. Fig. 1 also shows that curves for a fixed value of v are parallel but displaced vertically according to the value of the concentration factor C which

represents the number of particles restricting the visibility. Thus by relating the value of v and C to meteorological events it is possible to derive corresponding particle size distributions.

1.2.3 Exponential or Gamma Distribution

One disadvantage of the above described power law distribution function is that the curve is linear on a log log plot. This means that if a preferred concentration of particle sizes occurs then a peak would exist in the distribution and may not be well represented by the power law approach. Haze, fog, cloud, and rain particles often have a Pearson type III or log-normal distribution where the number of particles increases rapidly as particle radius increases and reaches a peak value after which there is a slower decay or trailing off of particles at increasingly larger sizes. The exponential or gamma distribution can handle these types of distributions but at the expense of greater complexity than the power law distribution.

A popular form of the exponential function is given by Deirmendjian as

$$n(r) = dN/dr = A\, r^{\alpha} \exp(-B r^{\gamma}) \qquad (4)$$

where n (r) units are $cm^{-3}\ \mu m^{-1}$, with particle radius r in micrometers, ans A, B, α, and γ being positive constants. Taking the derivative of Eq. (4) and settling it equal to zero gives the mode radius, r_c, that represents the radius of maximum concentration occuring at the peak of the size distribution curve and is expressed analytically as

$$r_c^{\gamma} = \alpha / B\gamma \qquad (5)$$

The concentration, N, or total number of particles per unit volume can be derived by taking the integral of Eq. (4) between the limits of zero and infinity to obtain

$$N = A\gamma^{-1} B^{-(\alpha+1)/\gamma} \Gamma\left(\frac{\alpha+1}{\gamma}\right) \qquad (6)$$

where Γ represents the gamma function. From this we can see that the coefficient A is proportional to the visibility or number concentration of atmospheric particles and is given by

$$A = N \gamma B^{(\alpha+1/\gamma)} / \Gamma(\alpha+1/\gamma) \qquad (7)$$

Most often γ is set equal to 1 for computation simplicity and to reduce Eq. (6) so that the gamma function is finite if $\alpha + 1 > 0$ and if $\alpha - 1$ is an integer then

$$\Gamma(\alpha + 1) = \alpha ! \qquad (8)$$

Thus with the above simplifications of $\gamma = 1$ and $\alpha + 1$ an integer, Equations (4), (5), (6), and (7) can be rewritten

$$n(r) = dN/dr = A r^{\alpha} \exp(-Br) \qquad (9)$$

$$r_c = \alpha / B \qquad (10)$$

$$N = A\alpha!\ B^{-(\alpha+1)} \qquad (11)$$

and

$$A = (N / \alpha !)\, B^{(\alpha + 1)} \tag{12}$$

Normally what is done is to select constant values for A, B, α, N, and r_c to represent static conditions for a given fog, cloud, or rain type in order to specify particular models to represent "average" particle size conditions. We are interested here in developing dynamical models of particle size distribution by turning the above so called "constants" into variables that are related to the type and changes of actual weather observations. Therefore let us now attempt to translate these "constants" in terms of meteorological variables.

The linear mean radius, r_m, is the sum of all the droplet radii divided by the total number of droplets so

$$r_m = \frac{1}{N} \int_0^{\infty} r \, n(r) \, dr \tag{13}$$

$$= \frac{1}{N} \, A \, \frac{(\alpha + 1)!}{B^{(\alpha + 2)}} \tag{14}$$

so

$$r_m = (\alpha + 1) / B \tag{15}$$

therefore

$$r_m = (\alpha + 1)\, r_c / \alpha \tag{16}$$

By definition the fog or cloud liquid water content, W_L, gives the total mass concentration of liquid water by

$$W_L \; (g \; m^{-3}) = 10^{-6} \, (4\pi / 3) \, \rho_w \int_0^{\infty} r^3 \, n(r) \, dr \tag{17}$$

where ρ_w is the density of water in g cm^{-3} and r is in micrometers. Expanding Eq. (17) gives

$$W_L = 10^{-6} \; (4\pi/3) \; \rho_w \; A \; (\alpha + 3)! \, / \, B^{(\alpha + 4)} \qquad (18)$$

Meteorologically speaking the density of water is essentially one g cm^{-3}, the liquid water content can be inferred from visibility observations in fog, the particle displacement along a moist adiabat in clouds, and the intensity for rainfall, and the coefficient B is defined by the mode radius as shown in Eq. (10). Thus we can solve for the coefficient A in Eq. (18) and obtain

$$A = 10^{+6} \; (4\pi/3)^{-1} \; (\alpha/r_c)^{(\alpha + 4)} \; W_L \, / \, (\alpha + 3)! \qquad (19)$$

Cloud and fog dropsize observations show that the mode radius r_c varies with such things as cloud or fog type, age, and height above cloud or fog base. Assuming we can reasonably approximate the mode radius and liquid water content then we are left with only the shape factor α as a variable needed before we can specify particle size distributions given by Eq. (9).

We have made a number of calculations to show how the particle size distribution changes according to individual changes in liquid water content, mode radius, and curve shape factor. First, Fig. 2 shows two different ways used to plot particle size distributions. The top log-log plot is a computer output solution of the above gamma equation for five

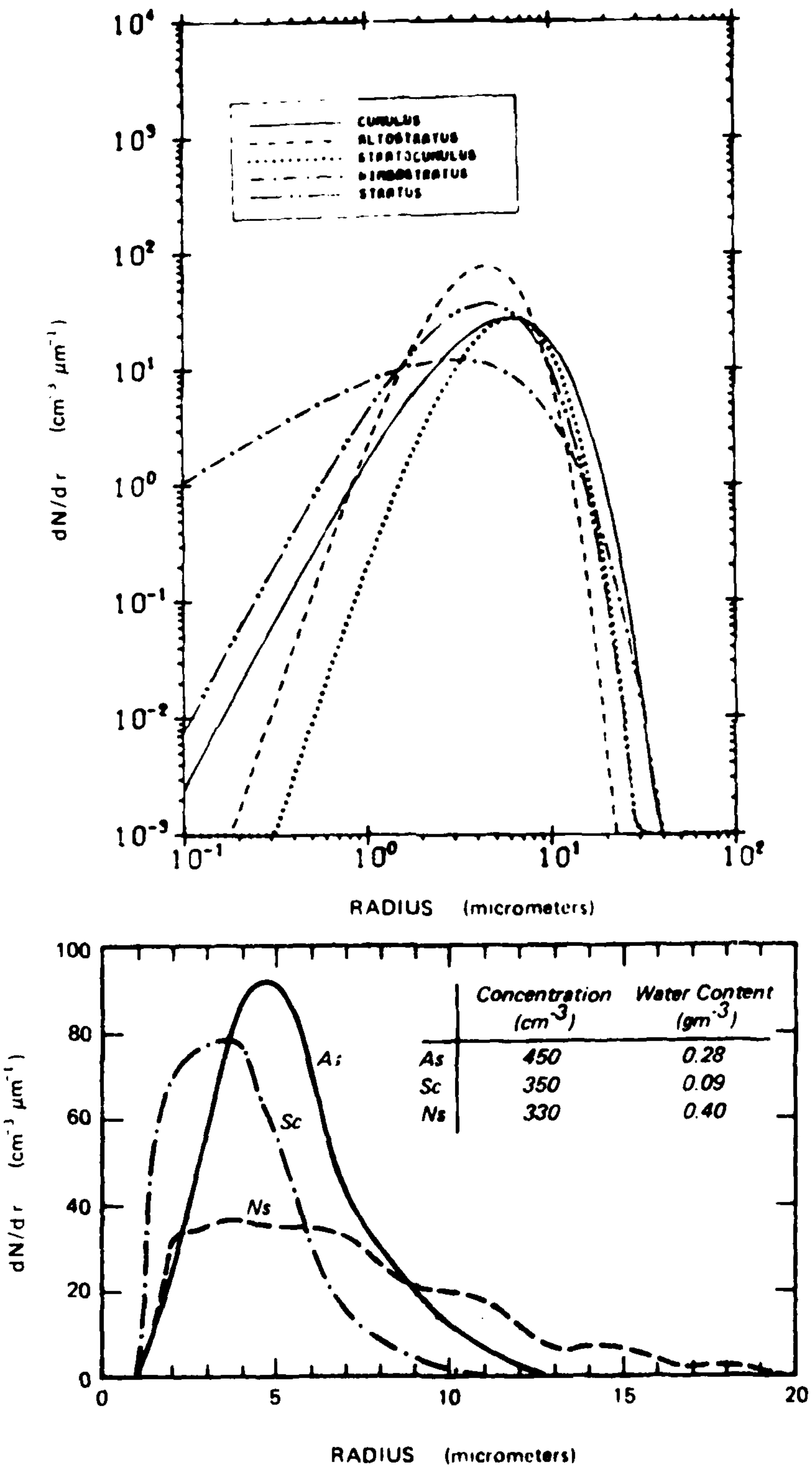

Fig. 2. Two Ways to Plot Cloud Particle Size Distributions.

different cloud types. The bottom linear plot of observed particles for altostratus (As), stratocumulus (Sc), and nimbostratus (Ns) clouds shows the familiar Pearson type III distribution. There is no preferred way to present such data. We will use mostly the log-log method because smaller concentrations of particles can be plotted with greater ease.

Figures 3, 4, and 5 show how the particle size distribution given by the exponential function varies when only one variable is allowed to change. Plots in Fig. 3 depict two orders of magnitude change in liquid water content while the mode radius, $r_c = 4\ \mu m$, and shape factor, $\alpha = 4$, remain constant. What is most striking in Fig. 3 is that the maximum density dN/dr varies from about 4.5 to 450 droplets per unit volume and radius interval (cm^{-3}, μm^{-1}) which represents significant differences in density of or visibility in clouds or fogs. Thus if we can infer the mode radius and shape factor for a specific type of fog or cloud then we can infer the number density of the droplets by obtaining a measure of the liquid water content.

We made calculations to show how variations in the shape factor coefficient α could be used to represent narrow or broad distributions in particle sizes. Fig. 4 shows, for a fixed liquid water content and mode radius, that as one selects higher and higher values for α one obtains sharper and sharper curves that represent a more narrow distribution of particle sizes. Also note that as the drop size distributions become broader, the number density decreases for the most frequently occurring particles while increasing for the small and large particles. Therefore, by knowing something about the variance or distribution of particle sizes associated with particular fogs or clouds it should be possible to select an appropriate shape factor.

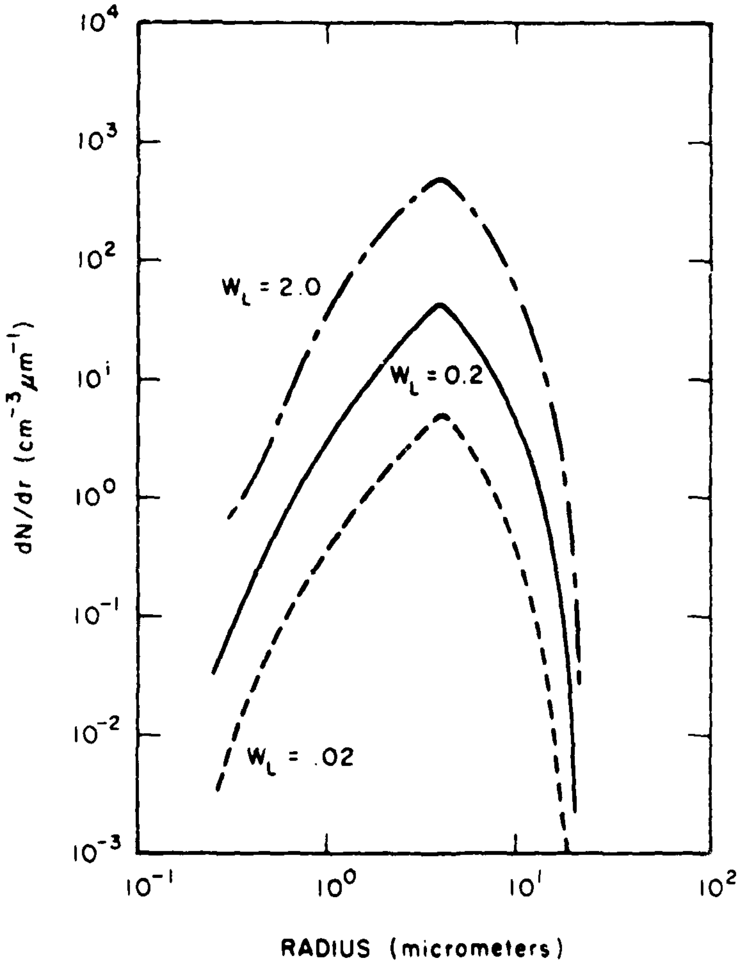

Fig. 3. Exponential Function Size Distributions For Three Liquid Water Contents, W_L= 0.02, 0.2, and 2.0 g m^{-3}, With Constant Mode Radius, r_C= 4 micrometers, and Shape Factor, α=4.

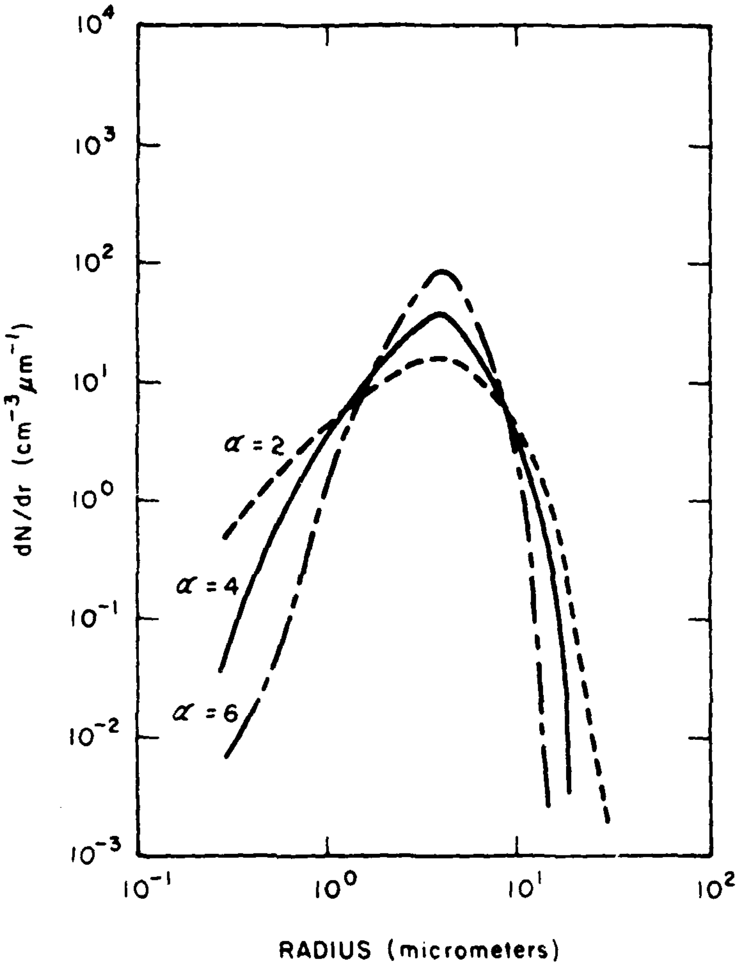

Fig. 4. Exponential Function, Size Distributions For Three Shape Factors, α= 2, 4, and 6, With Constant Liquid Water Content, W_L-0.2 gm^{-3}, and Mode Radius, r_c = 4 micrometers.

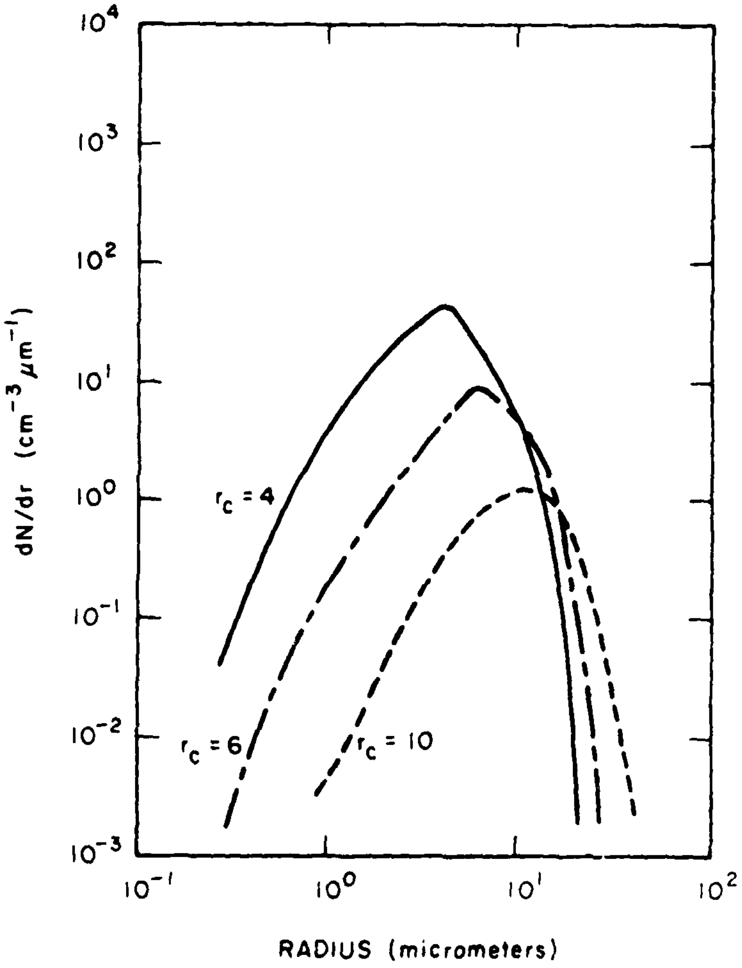

Fig. 5. Exponential Function Size Distributions For Three Mode Radii, r_c = 4, 6, and 10 micrometers, With Constant Liquid Water Content, W_L = 0.2 gm^{-3}, and Shape Factor, α = 4.

Lastly, we calculated droplet density for three environments where the most frequently occurring particle size was 4, 6, and 10 micrometers. During these computations, the liquid water content and shape factor were held constant. The results, Fig. 5, show the peak curve displacement corresponds with the selected mode radii and the peak number density of particles decreases as mode radius increases. Often a particular mode radius is representative of a particular type of fog or cloud. Thus by having information or observations on the liquid water content, the radius of the most frequently found droplet, and the variance or breath of particle sizes, we can select variables in the exponential or gamma function equation to depict a wide range of unimodal particle size distributions.

In the following report we will be using both the power law and exponential size distribution concepts described above to develop litho- and hydro-meteor models that can be specified given only routinely available weather observations.

2 DYNAMIC MODELS OF PARTICLE SIZES

2.1 LITHOMETEORS

2.1.1 Continential

2.1.1.1 Ground Level Variations

The underlying surface (land, ocean, vegetative, barren), soil type (humus, clay, rocky), soil condition (wet, dry, compacted, loose), atmospheric stability (convective, stable), and wind speed (soil erosion, vertical and horizontal advection) are important in determining type, concentration, and size distribution of lithometer particles as a function of space, time, and height in the atmosphere. To further complicate matters some dust grains are nonhydroscopic while others, especially salt containing particles, are highly hydroscopic. These hydroscopic particles include many well known things as salt from the sea, tars and resins from organic plants, smoke from industrial and battlefield fires, and the usual sulfate and nitrite chemicals from organic, combustion, and photochemical processes. The thing is, hydroscopic particles are not only important as light scatterers but also provide particle size changes as the ambient relative humidity approaches saturation and also provide the most active condensation nuclei needed in the cloud physics process of cloud/fog droplet and precipitation formation. In fact studies have been conducted to show light attenuation or visual range restriction as relative humidity increases, Fig. 6. The

important fact to us is that visual range or visibility is nearly linearly related to variations in relative humidity greater than about seventy per cent. That is to say that we

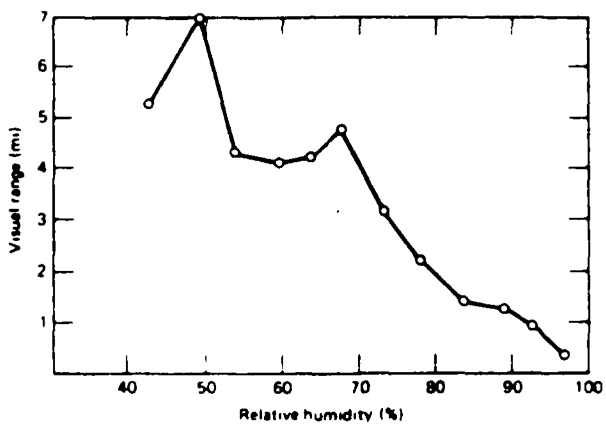

Fig. 6. Variation In Visual Range With Relative Humidity.

will consider variations in the particle size as a function of relative humidity to be incorporated in meteorological observations of visual range or visibility.

Dust particles, lithometeors, or haze are usually contained within the radius size range of 0.01 to 10 micrometers with a peak or most frequent particle radius of about 0.02 micrometers. There are two points of most interest to this study. First, most Army electro-optical systems are degraded or adversely effected by particle sizes equal to or greater than 0.1 micrometer in radius. Second, particle size observations at the earth's surface, at different geographical locations (Baltimore, Minneapolis, and Seattle) representing east - west coast and mid-sections of U.S.A., and day and night aerosol observations (Los Angeles) all show distributions

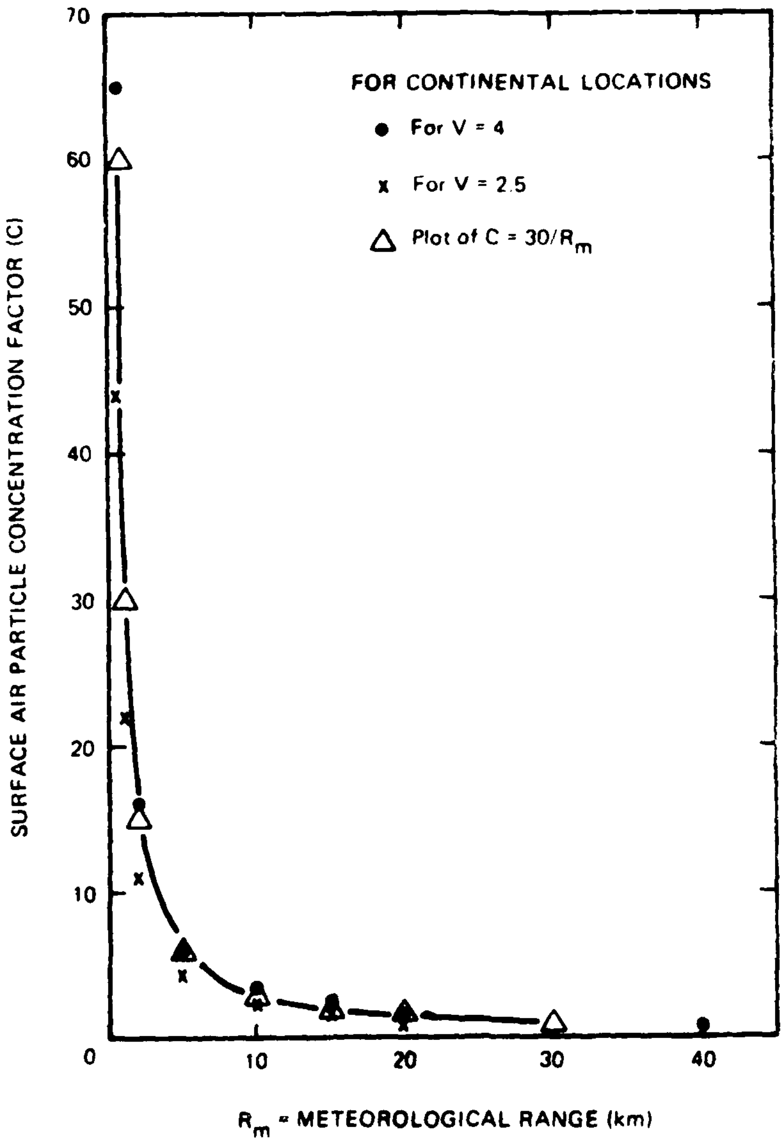

Fig. 7. Surface Air Haze Particle Concentration Factor Versus Meteorological Range.

having a r^{-4} dependence as given in Eq. (2). That is to say, the continental aerosol size distribution at the earth's surface follows a power law curve whose exponent is - 4. The exponent in Eq. (2) is $-(v + 1)$, therefore, a value of $v = 3$ is typical of ground level haze aerosols. The number density or vertical displacement of this curve, however, can vary considerably depending upon the number of particles suspended in the air at a given instant in time, which in turn is related to meteorological visibility.

Before Eq. (2) can be solved to derive the number density of haze aerosols it is necessary to obtain a measure of the particle concentration factor C. McCartney has shown that this concentration factor is directly proportional to the backscatter coefficient which in turn is proportional to the meteorological range, R_m, at optical wavelengths. We have plotted his values of the surface air particle concentration factor (C) as a function of meteorological range(R_m) in kilometers, see Fig. 7. McCartney presented data points for v in Eq. (2) equal to 2.5 and 4. From Fig. 7 it can be seen that our derived equation

$$C = 30/R_m \tag{20}$$

represents a reasonable fit to these data. More importantly, Eq.(20) allows us to use visibility observations reported over standard meteorological networks to infer variations in the number density of haze particles as weather conditions vary.

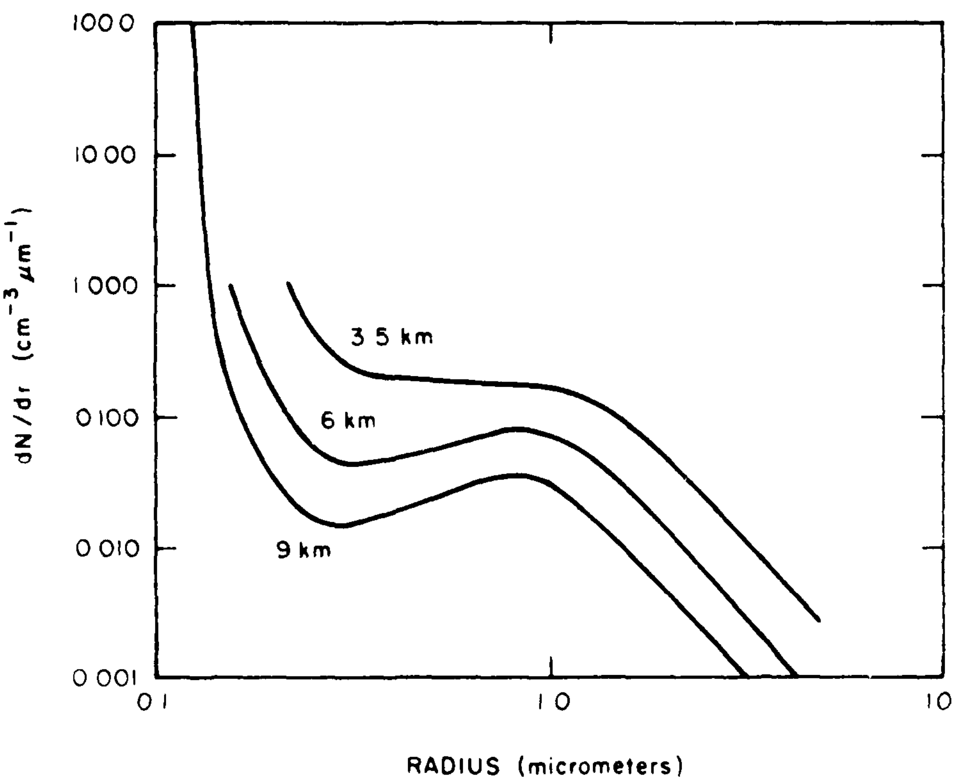

Fig. 8. Observations Over Death Valley.

2.1.1.2 Upper Level Variations

Aerosol variations with respect to geographical location and meteorological conditions decrease with height and often are considered to be non-existent near the troposphere, about 10 km. A bimodal distribution of aerosols is sometimes observed to increase with height above the earth's surface. In a static time dependent atmosphere it is not unusual for small particles to coagulate and form an ever-increasing size of lower concentration particles. There are, however, atmospheric regions where other forces retard this action and the maintenence or production of small particles remains high. Such appears to be the case in or around the tropopause height. This effect is shown in part by observations taken by Blifford (1970) over Death Valley, as shown in Fig. 8, for three different heights, namely 3.5, 6, and 9km. This figure also shows the gravitational settling effect on large particles so that a fewer number of larger particles exist at higher altitudes.

A great deal of dispersion exists among investigators in terms of what the vertical distribution is for atmospheric aerosol particle concentrations. This is clearly illustrated by Fig. 9. For example, the spread at 12km shows a dispersion of more than an order of magnitude. A typical "clear" atmospheric profile of aerosol concentration as a function of height is presented in Fig. 9 as plotted values of "C", which correspond to a clear atmosphere having a 23km range of visibility. Superimposed upon

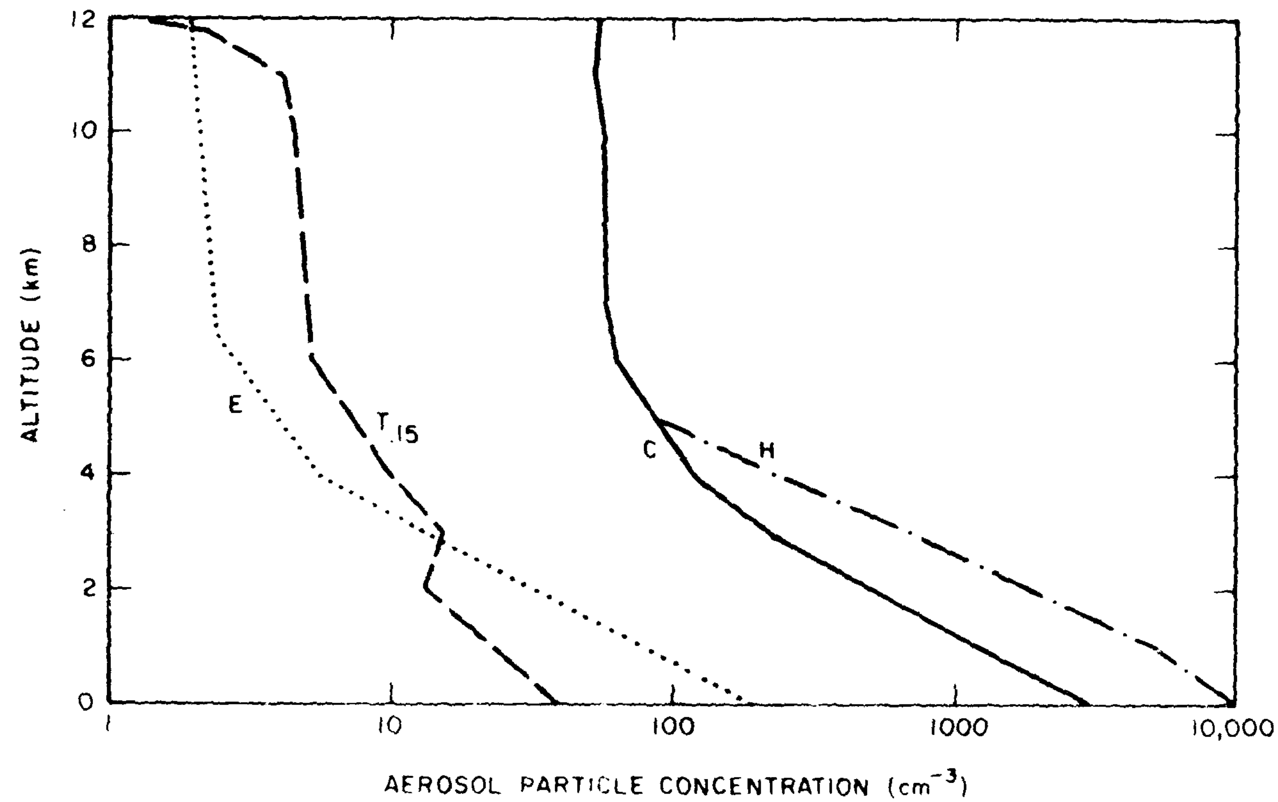

Fig. 9. Comparison of Vertical Variation of Aerosol Models.

this "clear" plot are a series of "H" values representing a hazy atmosphere whose influence extends from the ground surface to 5 km, above which the "hazy" and clear atmosphere have the same aerosol number concentrations. For this case, the hazy atmosphere corresponds with a ground level horizontal visibility of 5km. Also plotted for comparison is Toon's and Pollock's data ($T_{.15}$) for aerosol number concentrations for particles equal to or greater than 0.15 micrometers in radius that are found between the surface and 12km. Elterman's early data in 1964 resulted in a straight line in Fig. 9 extending from the surface to 10km, but more recent data in 1968 with better instrumentation displayed a break at 4 km with a small change or nearly constant value of particle concentration with height, see Fig. 9. As shown in Fig. 9, the hazy and clear models as well as the Elterman and Toon's data plots include those particle sizes that are most important in either remotely probing the atmosphere or studying optical or infrared radiational characteristics of the atmosphere. What is not shown, however, is how these particle size distributions change with height and changing weather environments.

We were looking for a measure of the change in particle size distribution as altitude increases above ground level. Blifford's balloon borne observations over Death Valley, Fig. 8, showed that the particle density not only decreased with height but so did the slope of the particle dis-

tribution curve. More recent aircraft data were collected over Western Europe by Cress, see Fig. 10, which showed similar results in that in general the observed distributions near the surface had a r^{-4} while those at about 5km had a r^{-2} slope. Cress plotted the exponent of r as the Junge Slope as a function of height and for spring, summer, and fall. We obtained a linear fit to the fall data, Fig. 11, and derived

$$v = 3 - Z / 2 \qquad (21)$$

where the Junge Slope = - (v + 1) as given in the power - law Eq. (2), and Z is the height about ground surface in km. The airborne equipment sampled aerosol sizes from 0.2 to 6 micrometers. Observations were taken under a wide range of meteorological conditions, including clear and overcast skies and visibilities varying from excellent down to 5km. A scatter of data points exists at all heights and should be expected due to physical variations previously discussed, e.q. underlying surface, atmospheric stability, wind, etc. Cress summer Junge Slope observations have about the same slope found in the fall data but the surface value for the Junge Slope is -5. This implies that the warmer and dryer underlying surface and more unstable boundary layer during summertime generates a larger number of smaller aerosols. The spring observations, Fig. 12, had a curvalinear distribution of Junge Slope with height and no one linear

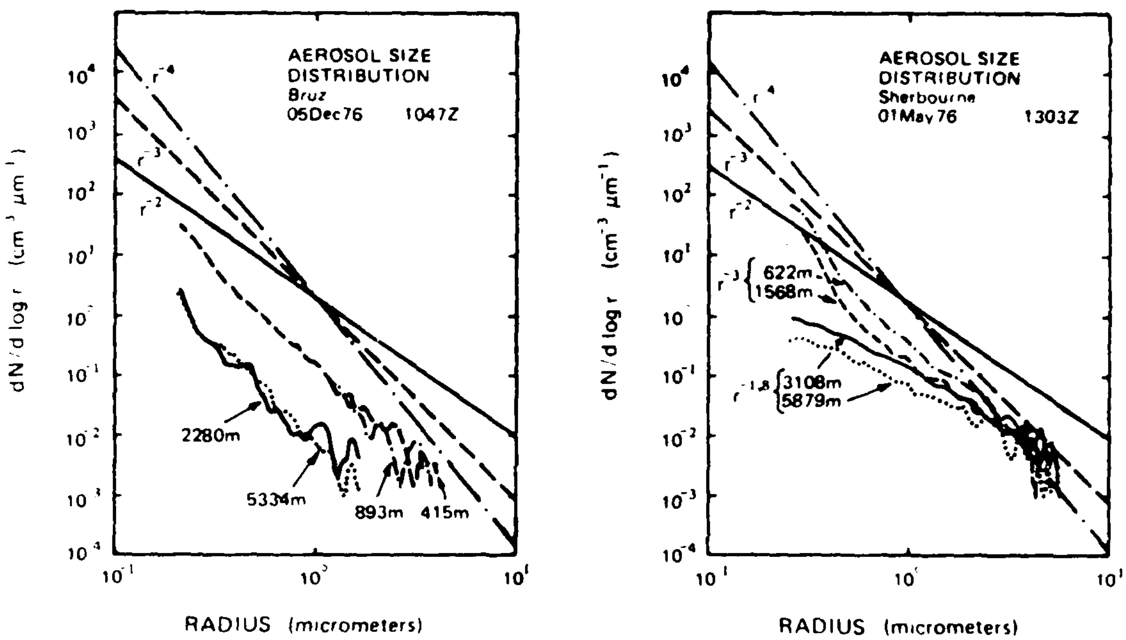

Fig.10. Aircraft Aerosol Observations at Different Heights.

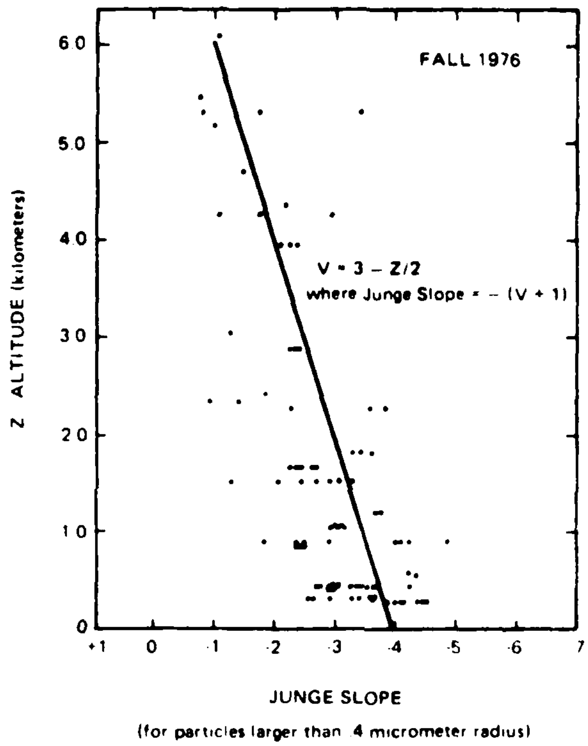

Fig.11. Fall Variation of Junge Slope With Height.

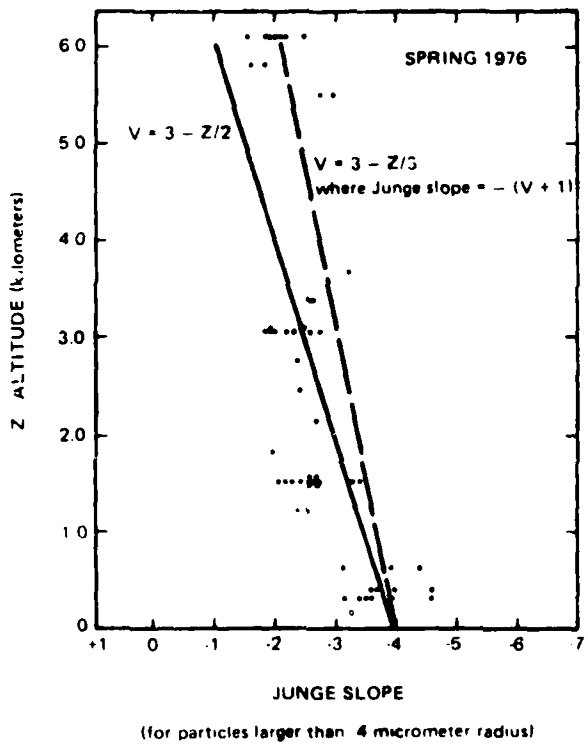

Fig.12. Spring Variation of Junge Slope With Height.

curve covers the entire range of data. For the fall and spring data a linear relation can be obtained between the surface and 4 km by using Eq. (21) and holding the Junge Slope constant at -2 for heights above 4 km. The same can be applied to the summer data so that the summer equation becomes

$$v = 4 - Z / 2 \qquad (22)$$

where again the Junge Slope = - (v + 1) as given in the power - law Eq. (2), and Z is the height above ground in km and can not exceed a value of 4km. At heights above 4km in summer v, equals a constant value of 2 so the Junge Slope remains constant at -3.

We now want to obtain an equation to describe the decrease in the total aerosol concentration with height. Fig. 9 shows two models and two data sets and, although they vary widely in the value for particle concentration at a specified level, they all show an exponential decrease with height from the surface to about 5km. Above that height, total particle concentration remains essentially constant up to the tropopause. In 1954 Penndorf derived

$$N_z = N_o \exp (- Z / H) \qquad (23)$$

to give the total number concentration of aerosols at a given height, N_z, as a function of the total concentration at ground level, N_o, the height in

the atmosphere in km, Z, and a term called the scale height in km, H. Penndorf's data suggested variations in H from 1.2 to 1.4 km. More recently in 1970, Elterman made simultaneous observations of meteorological range (R_m), optical attenuation coefficients, and aerosol scale height. In Fig. 13, we have plotted his data points and derived

$$H = 0.8 + R_m / 30 \tag{24}$$

where H and R_m are in km. This Eq. (24) applies for visibilities ranging from 0 to 18 km. The scale height remains constant at 1.4 km for visibilities greater than 18 km. By using Equations (23) and (24) it can be seen that as surface visibility increases the aerosol concentration with height decreases.

Thus it is possible to use the relations developed in this section to specify number density, concentration, and vertical distribution of aerosols as a function of routinely available weather data.

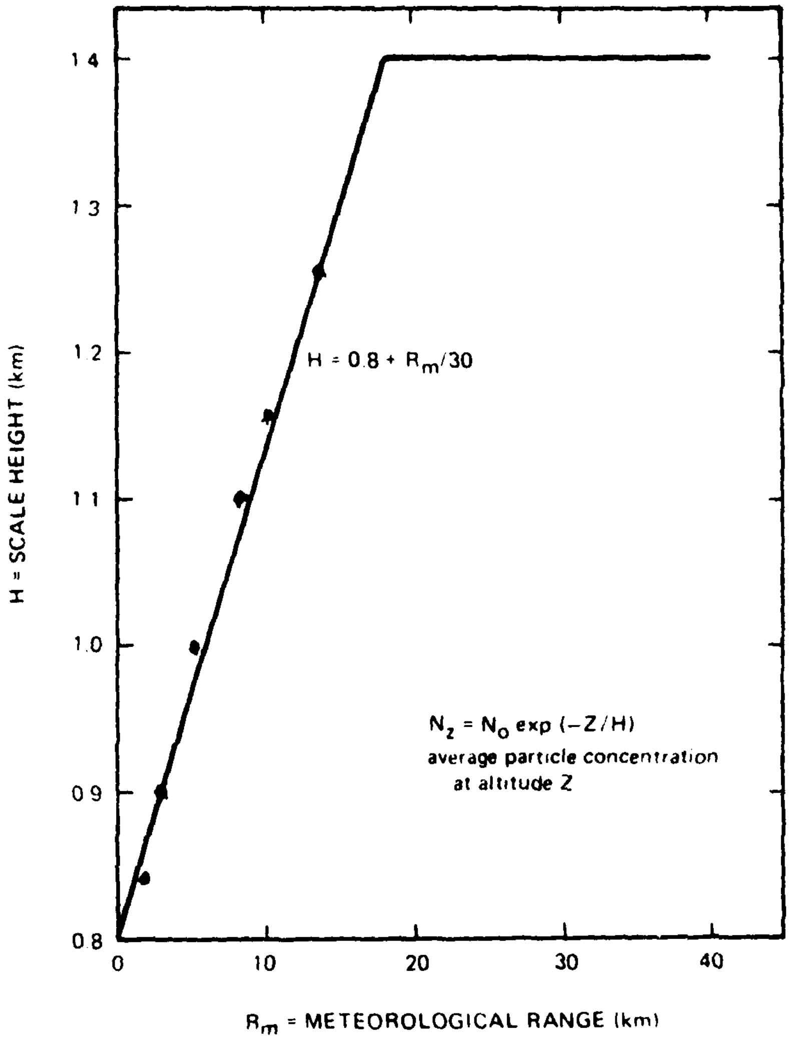

Fig. 13. Aerosol Scale Height Versus Meteorological Range.

2.1.1.3 Dynamic Procedure

Now we will present our sequence of steps taken to use standard meteorological observations to infer continental haze particle size distributions having radii equal to or greate. than 0.1 micrometer. These steps are:

1. Determine surface air particle concentration factor C from the observed meteorological range (R_m) in kilometers where $C = 30 / R_m$.

2. Derive the surface air particle size distribution using $n(Z,r) = \frac{dN}{dr} = 0.434 C r^{-(v+1)}$ where $n(Z,r)$ is in units of $cm^{-3}\ \mu m^{-1}$ and v is an exponential factor related to the type of aerosol and the altitude above the earth's surface. We found the haze exponential factor as a function of altitude Z in kilometers to be $v = 3 - Z/2$ for times other than summer months, which is valid from the surface to 4 km where v remains constant at one for higher altitudes. During summer months $v = 4 - Z/2$ from the surface to 4 km above which v remains constant at 2.

3. Determine the average particle concentration N(o,r) at the earth's surface by using the equations for C and n(Z,r) above and integrating the latter for spring and fall

conditions from r to infinity. Thus

$$N\ (o,r) = 0.434\ C\ (1/3)r^{-3}$$

For summer conditions

$$N\ (o,r) = 0.434\ C\ (1/4)r^{-4}$$

4. Compute the decrease in average particle concentration $N(Z,r)$ as altitude (in kilometers) increases above the ground using our empirical equation

$$N(Z,r) = N(o,r)\ \exp\ (-Z/H)$$

where H is the atmospheric scale height in km that varies with meteorological range as follows

$$H = 0.8 + R_m/30$$

where H reaches a constant value of 1.4 for very high visibilities (i.e. $R_m \geq 18$ km).

5. After deriving the average particle concentration at a particular height $N(Z,r)$, the size distribution value $n(Z,r)$ is

$$n(z,r) = v\ r^{-1}\ N(Z,r)$$

or

$$n(Z,r) = (3 - Z/2)\ r^{-1}\ N\ (Z,r) \quad \text{for spring and fall}$$

and

$$n(Z,r) = (4 - Z/2)\ r^{-1}\ N\ (Z,r) \quad \text{for summer}$$

where Z in the right hand side of the equations can never exceed 4 km.

Following the above steps, we made computations for aerosol size

distributions at 1.8 and 6.1 km to correspond with Cress's aircraft observations in western Europe, Fig. 14 and 15. Cress particle size measuring equipment was restricted to detections over the radius range from 0.2 to 6 μm. Considerable scatter exists in his observations which were taken over a wide variety of weather conditions ranging from clear to overcast skies and from excellent visibility down to a minimum of 5 km.

Now assuming the surface visibility is 20 km (the same as used in the AFGL Rural Model), the surface air particle concentration factor C equals 1.5 and the scale height equals 1.4. So the average particle concentration N(0,r) at the earth's surface is for spring and fall

$$N(0,r) = 0.434\ (1.5) \left(\frac{1}{3}\right) r^{-3}$$

$N(0,0.1) = 217\ cm^{-3}$ for particles $\geq 0.1\ \mu m$

$N(0,0.2) = 27.12\ cm^{-3}$ for 20 km visibility and particles $\geq 0.2\ \mu m$

$N(0,0.4) = 3.4\ cm^{-3}$ for particles $\geq 0.4\ \mu m$

and

$N(0,1.0) = 0.22\ cm^{-3}$ for 20 km visibility and particles $\geq 1.0\ \mu m$

At an altitude of 1.8 km then

$$N(1.8,r) = N(0,r)\ e^{-\left(\frac{1.8}{1.4}\right)}$$

$N(1.8,0.1)\ 60.0\ cm^{-3}$ for particles $\geq 0.1\ \mu m$

$N(1.8,0.2)\ 7.50\ cm^{-3}$ for particles $\geq 0.2\ \mu m$

$N(1.8,0.4)\ 0.94\ cm^{-3}$ for particles $\geq 0.4\ \mu m$

$N(1.8,1.0)\ 0.06\ cm^{-3}$ for particles $\geq 1.0\ \mu m$

then

$$n(1.8,r) = \left(3 - \frac{Z}{2}\right) r^{-1} \quad N(1.8,r)$$

$$n(1.8,0.2) = 78.8 \text{ cm}^{-3} \ \mu\text{m}^{-1} \text{ for } r = 0.2 \ \mu\text{m}$$

$$n(1.8,1.0) = 0.13 \text{ cm}^{-3} \ \mu\text{m}^{-1} \text{ for } r = 1.0 \ \mu\text{m}$$

At an altitude of 6.1 km, where Cress aircraft observations were taken over western Europe, and assuming a 20 km surface visibility then

$$N(6.1,0.2) = 0.35 \text{ cm}^{-3} \text{ for particles } \geq 0.2 \ \mu\text{m}$$

$$N(6.1,1.0) = 0.003 \text{ cm}^{-3} \text{ for particles } \geq 1.0 \ \mu\text{m}$$

and

$$n(6.1,0.2) = 1.75 \text{ cm}^{-3} \ \mu\text{m}^{-1} \text{ for } r = 0.2 \ \mu\text{m}$$

$$n(6.1,1.0) = 0.003 \text{ cm}^{-3} \ \mu\text{m}^{-1} \text{ for } r = 1.0 \ \mu\text{m}$$

Since from Eqs. (1) and (2) $dN/d \log r = (r/0.434)\, n(Z,r)$ then at 1.8 km

$$dN/d \log r = 36.3 \text{ cm}^{-3} \ \mu\text{m}^{-1} \text{ for } r = 0.2 \ \mu\text{m}$$

$$dN/d \log r = 0.3 \text{ cm}^{-3} \ \mu\text{m}^{-1} \text{ for } r = 1.0 \ \mu\text{m}$$

then at 6.1 km

$$dN/d \log r = 0.81 \text{ cm}^{-3} \ \mu\text{m}^{-1} \text{ for } r = 0.2 \ \mu\text{m}$$

$$dN/d \log r = 0.007 \text{ cm}^{-3} \ \mu\text{m}^{-1} \text{ for } r = 1.0 \ \mu\text{m}$$

In order to provide a means for comparison with our GAC Model, plots are shown in Figs. 14 and 15 for Cress's aircraft data, Blifford's impactor data, and two models of the Air Force Geophysics Laboratory (AFGL) i.e., AFGL tropospheric Model and the AFGL Rural Model for a 20 km visibility. It can be seen that the GAC Model provides the best fit.

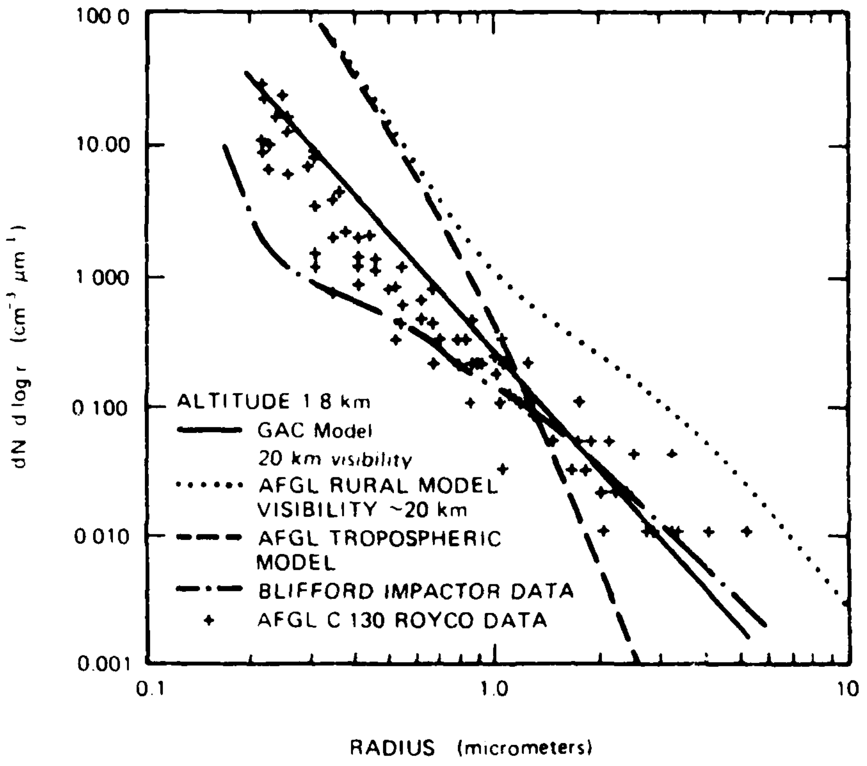

Fig. 14. Comparison of Aerosol Models at 1.8 km.

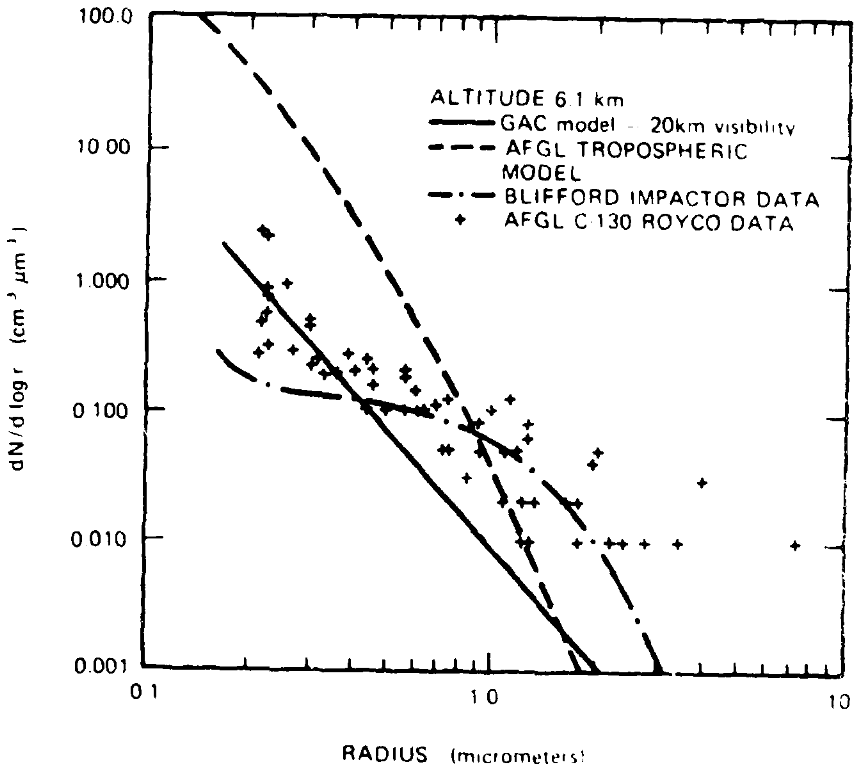

Fig. 15. Comparison of Aerosol Models at 6.1 km.

2.2 HYDROMETEORS

2.2.1 Fog

2.2.1.1 Ground and Upper Level Variations

This section on hydrometeors will cover fog, cloud, and rain drop size distributions. An overview of these features can be obtained from Fig. 16 where it shows about a 12 order of magnitude change in number density and about half that change for representing the possible range in droplet radii. Often in the real world there is a number of possible combinations of hydro - and litho- meteors occuring simultaneously. High pressure regions with clear skies and stable boundary layers are condusive to good radiational cooling and fog formation. Also it is not unreasonable to expect trapping of haze particles in the stable surface air layer and to have a mixture of both haze and fog particles. Other event combinations occur, such as drizzle and fog, yet we tend to focus our modelling efforts on a simple event representation. That is also done here, however, provisions are made and results shown to combine outputs from multi models to better simulate all reported weather.

Many types of fog exist to produce large spatial and temporal variations in "seeability." Recent improvements and technology advances in both particle sampling and sizing instruments and observational platforms needs to be exploited in carefully conceived and implemented field ex-

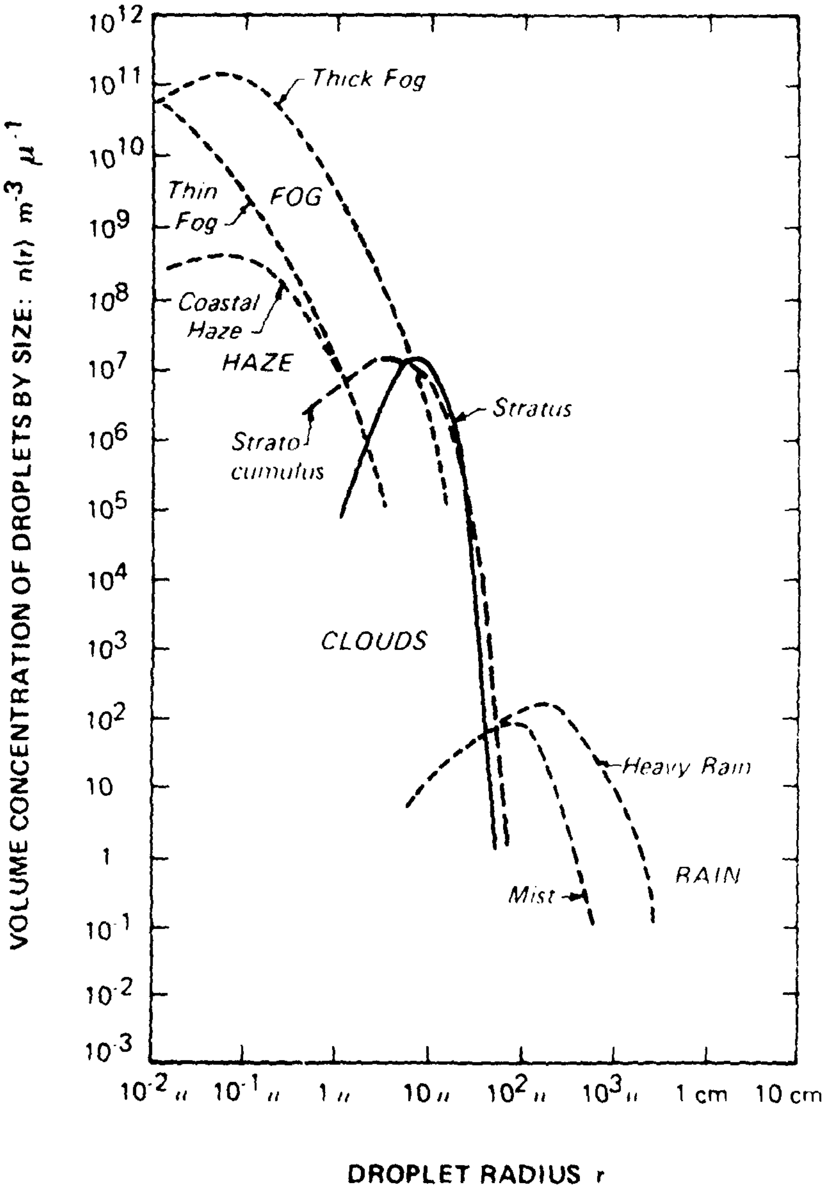

Fig. 16. **Volume Concentration of Water Droplets by Size (Counted in 1-μm Intervals of Droplet Radius)**

perimental and data analysis programs. Such data are basic to defining microphysical structure as well as to generating synoptic and mesoscale models as done here.

Fog conditions often go through three distinct stages, i.e. initial oscillatory, steady dense, and break up stage. Particle sizes during the initial oscillatory stage usually have a narrow range of values, the most frequently occuring radius is small, the liquid water content is less, and haze and fog particles combine to weight the size distribution to smaller sizes. Dense persistent fogs are older in character, having higher liquid water content, broader range of particle sizes, larger mode radius, and greater EO attenuation. The break up stage depends greatly upon the fog type, formation, density, thickness, and physical processes producing the break up. The particle size distribution of breaking-up fog reverts back more to a haze like character with an ever decreasing residual peak in the concentration of the larger mode radius. Typical fog parameters are shown in the following Table 2.

Table 2. Typical Fog Parameters

Parameter	Fog type			
	Radiation (new)	Radiation (old)	Valley	Advection
mode radius (μm)	4	10	8	10
breath of size distribution	narrowest	broad	broad	broadest
vertical depth (m)	variable	200	150	400

The time period that usually separates new from old fogs is on the order of 2 hours after formation. Several other names have been used to describe these fog types. For example newly formed fogs are sometimes called "selective fog." Older or dissipating fogs may be called "stable fog" or "evolving fog." Likewise advection fog near the sea shore is called "coastal fog." Often "low mountain fog" is called valley fog and stratus clouds intersecting a mountain are called "high mountain fog." We know the preferred mode radius of fog has seasonal, geographical, and meteorological variations that need better definition. Until these refined data become available, for our purpose, the above listed mode radius will be used.

Liquid water content of a fog must be specified in order to define the fog density or concentration of droplets. Sensors do exist for directly measuring liquid water content and these are the most accurate and reliable but are not too feasible within a battlefield environment. Horizontal visibility observations are available from routine and nonstandard observational sources and may be used to infer liquid water content of fog. A number of experimental studies have been made of liquid water content and atmospheric visibility. We have averaged some of these results and plotted three curves in Fig. 17 to depict liquid water content versus visibility for coastal fog and two inland fog types (new and old). The equations used in this study

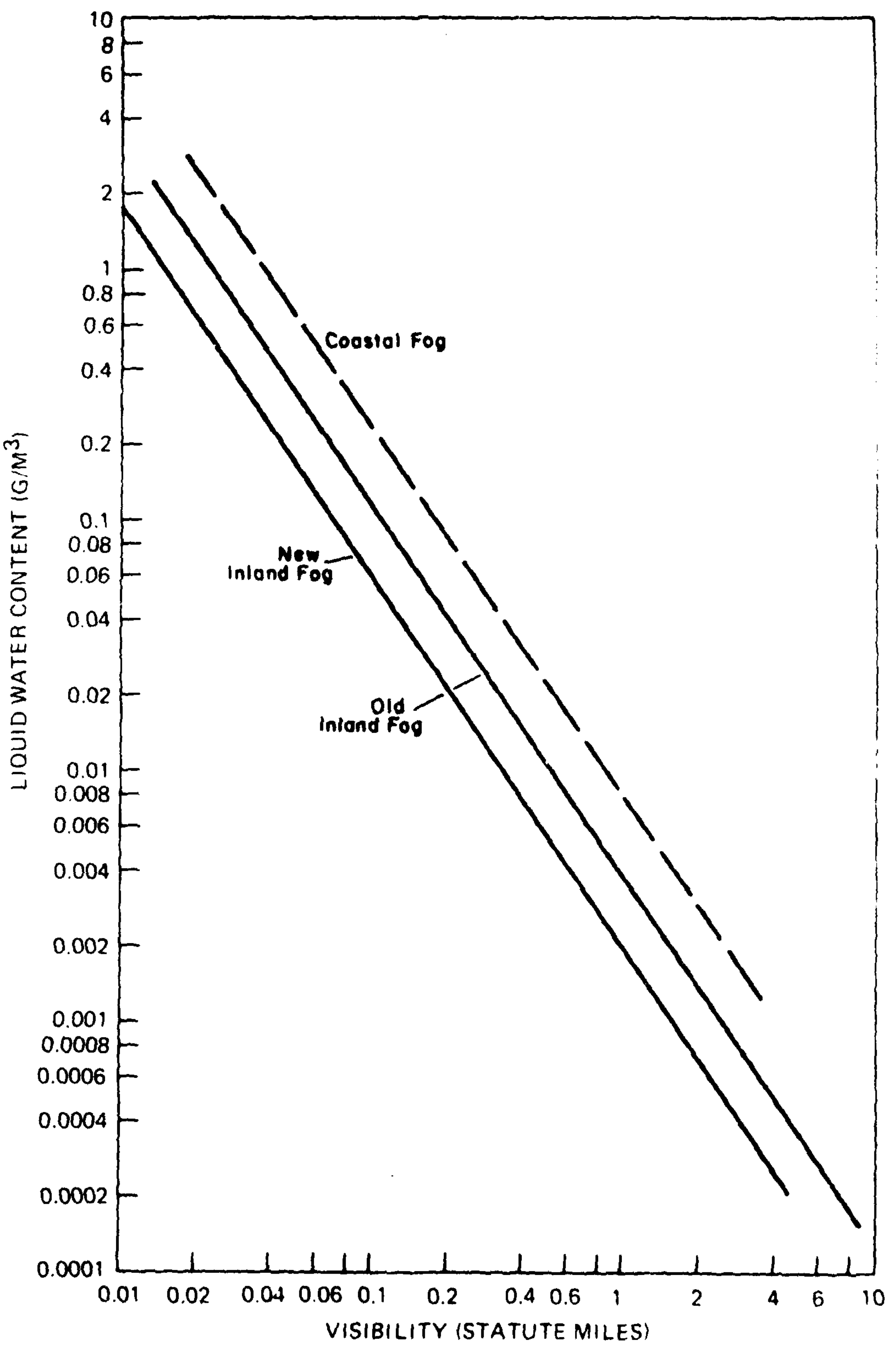

Fig. 17. Relationship between Visibility and Liquid Water Content in Fog

to derive fog liquid water content, W_L in g m^{-3} as a function of meteorological visual range, R_m in miles, are

<u>Coastal Fog</u> $$W_L = (27.15\ R_m)^{-1.43} \tag{25}$$

<u>Inland Fog</u>

<u>Old</u> $$W_L = (41.7\ R_m)^{-1.54} \tag{26}$$

<u>New</u> $$W_L = (58.8\ R_m)^{-1.54} \tag{27}$$

By comparing information from Table 2 and Fig. 17 it can be seen that the narrowness or breath of drop size distributions is dependent on fog type which in turn is related to liquid water content. That is to say that for a fixed visibility, liquid water content is higher and the drop size distribution broader for coastal than for either inland fog types. In order for modelling techniques to be representative the exponential function shape factor α must vary as fog density varies to produce a size distribution which is very narrow (where α is large) when the liquid water content is low and very broad (where α is small) when liquid water content is high. We analyzed a wide variety of droplet size distributions to obtain the following shape factor relationship

$$\alpha = 1 - 1.4 \ \ln W_L \tag{28}$$

where W_L is the fog liquid water content in g m^{-3}. For computational

simplicity and so that our equations in section 1 of this report would not have to increase in complexity, we placed two restrictions on the value of α, first it can never be less than one, and second it must be rounded off if necessary to be a whole integer.

The composition of inland fog normally varies with height above ground level. The number of fog droplets per unit volume usually increases from the ground to the top of the fog. Larger droplets and higher liquid water content are usually found at the base of inland fogs whereas coastal fogs are more homogeneous in the vertical. For older and more stable inland fogs the drop size distributions become more narrow and unimodal and the mean radius decreases with increasing altitude above the surface. For a composite of old inland radiational and valley fogs we found average vertical variations for mode radius r_c and liquid water content W_L to be

$$d\ r_c\ /\ d\ Z = -\ 1\ \mu m\ /\ 100\ \text{feet} \tag{29}$$

and

$$d\ W_L\ /\ d\ Z = -\ 0.4\ g\ m^{-3}\ /\ 100\ \text{feet} \tag{30}$$

with a minimum value of 4 μm applicable to r_c. Observations of coastal, advection, or marine fogs often show nearly constant or increasing liquid water content with increasing height in the fog. For this paper we will assume constant conditions prevail from the surface to the top of coastal fogs.

2.2.1.2 Dynamic Procedure

1. Use the output of analyses of meteorological surface and upper air observations, such as our CFAS (Cloud Fog Analysis System) or our CIVAS (Cloud/Icing/Visibility Analysis System), to identify the type, age, and thickness of fog, other restrictions to visibility such as haze, mist, etc., and the visibility.
2. Select the applicable mode radii r_c from Table 2.
3. Derive the ground level liquid water content from either Eqs. (25), (26), or (27).
4. Compute the shape factor from Eq. (28).
5. Obtain the coefficient A from Eq. (19).
6. Derive the B coefficient from Eq. (10).
7. Determine the particle size distribution n(r) from Eq. (9).
8. Derive the total nimber concentration of droplets for all radii using Eq. (11).
9. Plot the output of steps 7 and 8 to depict surface level fog droplet conditions.
10. Determine if other constituents are also restricting the visibility and solve for and incorporate their contributions to the overall particle size distribution.
11. Derive the vertical variation of r_c and W_L from Eqs. (29) and (30) and incorporate and repeat step 4 through 10 to obtain particle

size distribution at any desired level within the fog layer.

Using the above steps we computed particle size distribution for observations (Jiusto 1979) of haze and radiation fog. Meyer's (1980) data showed that a good linear relation exists between visual ranges equal to or greater than 5 km and the cumulative number concentration of haze particles. The number concentration almost remains constant for haze/fog conditions with visual ranges from 1 to 5 km. For visual ranges less than about 1 km a linear relation exists between the number concentration and visual range in dense fog. Therefore, for fog and haze conditions, the haze component of particle size distribution was computed for a visual range of 5 km and was held constant and added to the fog contribution which varied with visual range. Our results are shown in Fig. 18 for two reported visibilities, 2.1 and 0,39 km. For comparison, observed size distributions are shown for three observation times 0725, 0730 and 0800 and visibilities 2.1, 1.4, and 0.39 km, respectively. It is striking, however, how good the major features and time trends are represented by our haze/fog model.

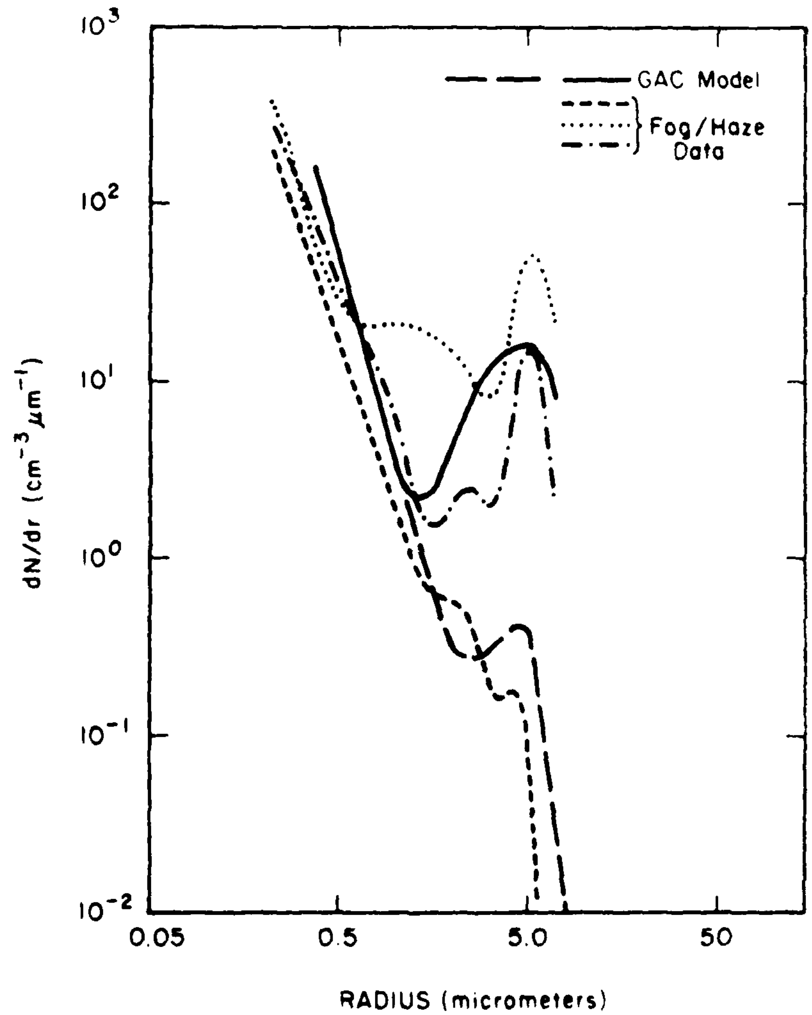

Fig. 18. GAC Haze-Fog Model Compared With Observed Data

2.2.2 Cloud

2.2.2.1 Cloud Base and In Cloud Variations

We have had a great deal of difficulty looking for common denominators that are applicable to the many cloud physics studies. This is due in part to the fact that most investigators direct their attention to one particular cloud type and then do not measure all variables important to a more generalized study. For example, Table 1 shows that for a particular cloud type there is a most frequent particle radius that occurs on the average for all seasons and types of conditions. Yet it is not unreasonable to expect that cloud particles and their distribution are dependent upon the environment in which they are formed. We have tried to take these features into account from a meso- and synoptic-scale point of view, knowing full well that certain micro-scale features must either be neglected, averaged, or inferred from current observations.

Our desire is to be able to derive cloud characteristics at the cloud base and heights within the cloud, given only standard meteorological observations.

We have found that clouds formed primarily by convection (cumulus and cumulonimbus), turbulence (Stratus, stratocumulus, and altocumulus) and horizontal convergence (altostratus, as well as altocumulus) exhibit distinctive features but, most often when looked at in detail, their microphysics is dictated by the temperature, pressure, dew point, and vertical motion that exists

at the cloud base and levels within the cloud. That is to say, originally it was thought that each cloud type would have to be treated separately. Now, however, we found that cloud base characteristics and their vertical variation within a cloud could be formulated using the most recent surface and upper air observation.

Lewis (1951) compiled tables displaying cloud droplet and liquid water content for a large number of aircraft observations segmented into three broad cloud type categories, i.e. stratus and stratocumulus, alto-stratus and alto-cumulus, and cumulus or cumulonimbus. Separating these categories geographically between the Pacific Coast and other regions of the United States showed that in general cloud drops for corresponding west coast cloud types are about 2 micrometers larger in radius. Although cloud base temperature and to a lesser extent the cloud base pressure height contribute to changes in the mean particle size we were unsure whether sufficient differences existed between clouds on the Pacific Coast versus those in Eastern U.S.A. We used data prepared by the Naval Weather Service in 1976 on "Climatic Study of the Near Coastal Zone" from two publications, "East Coast of the United States" and "West Coast of the United States." On the average the surface air temperature is 10°F warmer in the winter at San Francisco than at Philidelphia and the reverse in summer, so the yearly surface air temperatures are about the same value. More important, however, is that the west coast

clouds occur significantly more frequently at lower heights with warmer cloud base temperatures. This is especially noticeable during the winter when most of the clouds exist and when more than 50 per cent of the west coast clouds have a ceiling height of less than 1000 feet whereas only 15 per cent are found at the same low levels on the east coast. We also analyzed Selby's drop size measurements in low level stratus in another country, England, (Blifford 1970). This was interesting since most of the individual cases gave a mode radius of 2 micrometers for cloud droplets within the lower 30 to 60 meters of their stratus clouds. Such small droplets near the cloud base are reported more frequently in the later literature as instrument measuring technology improved. The main point is that major features of these liquid clouds from wide geographical locations were found to be represented by our following procedures. Spatial distribution of the microstructure of cloud liquid water content varies considerably in both horizontal and vertical directions. This is especially true for convective type storms where vertical cloud development is more pronounced, vertical motions are higher, the total cloud cellular structure is often composed of a combination of individual sub cells, and the turbulent motions produce more entrainment of drier ambient air which reduces the available liquid water and causes gradients in the actual liquid water content. A possibility does exist to use remote probing techniques to better define the actual cloud microstructure. However, since this study is

restricted to using standard surface and upper air observations, we have to develop techniques to depict major features associated with these meso-scale phenomena. Using information contained in our CIVAS (cloud/icing visibility analysis system) we can specify the cloud base height and temperature, cloud type, and vertical and horizontal extent. From this we can compute the available liquid water content produced by cloud air rising along its moist adiabatic lapse rate. This approach produces the amount of liquid water that can be expected at each level in the cloud. As discussed above some of this water has to go to injecting moisture into the dry entrained air to bring it to saturation and thus the actual liquid water contained at any cloud level is less than that expected from purely adiabatic processes. Furthermore this effect and moisture reduction increases with altitude in the cloud. A number of cloud physics studies have been made showing the changes of the ratio of actual cloud liquid water to that expected adiabatically as a function of height above the cloud base, Pruppacher (1980). In general the actual liquid water is a high percentage of that available near the cloud base and decreases to nearly a quarter of that available by one kilometer above the cloud base and remains essentially constant at higher cloud levels. We have fitted these data with a linear curve covering the first kilometer of the cloud and a constant value of 0.2 for the liquid water content ratio at higher levels in the cloud. The equations are

and

$$W_L / W_{AL} = 1 - 0.8\ Z_{ACB} \quad \text{for } Z_{ACB} = 0 \text{ to } 1 \text{ km} \tag{31}$$

$$W_L / W_{AL} = 0.2 \quad \text{for } Z_{ACB} > 1 \text{ km} \tag{32}$$

where Z is the height in km above the cloud base and the ratio is the cloud liquid water content (W_L) relative to the cloud liquid water content available (W_{AL}) through moist adiabatic processes. This information will be combined with other cloud characteristics to obtain a measure of size distribution and number concentration of cloud droplets at different heights in the cloud.

Complicated equations are necessary to precisely derive the complicated pseudoadiabatic lapse rate as a function of temperature and pressure at the cloud condensation level, including both the liquid or ice stage of the cloud. Another set of equations is necessary to derive the saturation mixing ratio over water and over ice as a function of air temperature and pressure within the clouds. By incrementally solving these equations it is possible to derive the available liquid water at each level in a cloud. This precision is unwarranted at this time. Considering the uncertainties in other approximations to depicting cloud microphysical features, we have derived the following simplified equations to derive the available liquid water concentration, W_{AL}, produced by moist adiabatically lifted air

for the first kilometer in the cloud

$$W_{AL} = (1.42 + 0.05\ T_{CB})\quad Z_{ACB} \tag{33}$$

and for heights greater than one kilometer above cloud base

$$W_{AL} = 1.42 + 0.05\ T_{CB} + (0.84 + 0.035\ T_{CB})(Z_{ACB} - 1) \tag{34}$$

where W_{AL} is in g m^{-3}, T_{CB} is the cloud base temperature in ^{o}C and Z_{ACB} is the height above cloud base in km.

Next we wanted to obtain a quantitative method to derive the mode radius r_c since this is a necessary variable in utilizing the previously described exponential distribution. The peak radius of a size distribution curve was found to be directly proportional to the amount of liquid water and the cloud base temperature. We empirically derived

$$r_c = \left(\frac{3.17 \times 10^4\ W_L}{340 - 8\ T_{CB}}\right)^{1/3} \tag{35}$$

where r_c is the mode radius in micrometers, W_L is the cloud liquid water content in g m^{-3}, and T_{CB} is the cloud base temperature in ^{o}C. This equation was derived assuming a shape factor $\alpha = 2$ and using continential cumulus cloud data to derive $N = 340 - 8\ T_{CB}$ in order to relate the average total cloud base droplet concentration to cloud base temperature. Because of the limited time available for this study, this equation was then used for all cloud types. In order to derive the mode radius at the cloud

base, we assumed no entrainment within the first tenth of a kilometer of the cloud to derive W_L, which is then dependent only upon the cloud base temperature. Therefore, the mode radius r_c at any cloud base is given only by the cloud base temperature, producing mode radii equal to 2.8, 3.5, and 4.5 micrometers for cloud base temperatures of 10, 20 and 30°C respectively.

We then explored two methods to depict vertical changes of the mode radius within a cloud. We used aircraft observations, Blifford 1970, of summer cumulus and obtained the following best fit equation

$$r_{c,Z} = r_{c,Z_{CB}} + 2.3\ Z_{ACB} \tag{36}$$

where $r_{c,Z}$ and $r_{c,Z_{CB}}$ is the mode radius at any height Z within the cloud and at the height Z_{CB} of the cloud base, respectively, and Z_{ACB} is the height in kilometers above cloud base. The other method was to use the above equations to derive liquid content and mode radius at any given height within a cloud of known base temperature. Also used was Eq. (28) to derive the shape factor α, Eqs. (10) and (12) to derive the B and A coefficients, and Eq. (11) to derive the total droplet concentration N per cubic centimeter volume. Before looking at detailed comparisons of computed versus observed droplet characteristics as a function of height within a cloud, we will look at comparisons with more grossly averaged cloud characteristics.

Observations from 5 different investigators (aufm Kampe & Weickman 1957) were combined to produce a frequency distribution of mean linear droplet radius and water content for layer (stratus) clouds, fair weather cumulus, and cumulus congestus or cumulonimbus. We assumed an average cloud base temperature of 15°C and used the observed liquid water content to compute the expected mode radius. The results are:

Cloud Type	Observed liquid water	Observed mean radius	mode radius	Computed mode radius	difference
stratus	0.15	5.5	3.7	2.8	0.9
fair weather cumulus	0.6	5.5	3.7	4.4	0.7
cumulonimbus	2.4	12.5	8.3	6.9	1.4

The internal microphysical structure of layer clouds (aufm Kampe & Weickman 1957) was subjected to the same analysis and assumptions as above to obtain averaged conditions for the base, middle, and top of these clouds. The results are:

Cloud Type	Location	Observed liquid water	Observed mean radius	mode radius	Computed mode radius	difference
stratus	base	0.03	5.5	3.7	1.6	2.1
nimbostratus	middle	0.15	5.5	3.7	2.8	0.9
	top	0.3	8.4	5.5	3.5	2.0
stratocumulus	base	0.15	5.5	3.7	2.8	0.9

Cloud Type (cont.)	Location	liquid water	Observed mean radius	mode radius	Computed mode radius	difference
altocumulus	middle	0.30	5.5	3.7	3.5	0.2
(altostratus)	top	0.15	5.5	3.7	2.8	0.9

It is interesting that the differences between computed and observed mode radius are about one micrometer for almost all cloud types, except stratus where computed values are about two micrometers too small.

We looked at greater vertical detail of cumulus cloud observations (aufm Kampe & Weickman 1957) and used both methods described above to compute expected conditions. In this case the average cloud base temperature was 25^{o}C and we obtained the following comparisons for cumulus clouds:

Height Within Cloud	Observed r_c	W_L	N	Computed "A" r_c	W_L	N	Computed "B" r_c	W_L	N
base	2.0	0.15	330	3.8	0.25	246	3.8	0.25	246
1 km	9.2	1.0	150	4.8	0.53	153	6.1	0.53	74
3 km	9.9	2.8	60	6.4	1.22	50	10.7	1.22	10
5 km	7.9	2.0	50	7.4	1.91	52	15.3	1.91	13

where computed "B" uses empirical Eq. (36) relating mode radius as a function of only initial conditions at cloud base and height above it where as computed "A" uses the computed vertical distribution of liquid water and

the corresponding shape factor and mode radius for a given cloud base temperature. In all cases, total particle number content is best obtained at all levels within a cumulus cloud by using method "A", whereas in most cases method "B" provides the best representation of the mode radius. The liquid water content is computed the same for both methods and is always somewhat smaller than observed. This implies our entrainment equation is exerting slightly greater influence than required for this case. Actually, with a higher liquid water content computed, a larger mode radius would be computed and method "A" would be most applicable overall.

2.2.2.2 Dynamic Procedure

1. Using objective surface and upper air analysis techniques, such as CIVAS, obtain cloud type, cloud base temperature, cloud height above ground level, and horizontal and vertical extent.
2. Compute the liquid water content applicable at or near the cloud base using Eq. (33) with $Z_{ACB} = 0.1$ km.
3. Combine the cloud base temperature and liquid water content in Eq. (35) to derive expected cloud base droplet mode radius.
4. Derive the cloud liquid water content as a function height in the cloud by applying either Eqs. (33) or (34) and applying the entrainment factor Equations (31) or (32), depending upon height above cloud base.
5. Determine the exponential shape factor using Eq. (28) at each desired height in the cloud where liquid water content was computed.
6. Use Eqs. (9), (10), (11), and (12) to derive the details of the number concentration and drop size distribution as a function of horizontal and vertical distance within the cloud.

2.2.3 Rain

2.2.3.1 Ground and Upper Level Variations

Wartime radar research provided special urgency in measuring raindrop size distribution. In 1943 Laws and Parsons began a new approach to the problem by collecting raindrop size data and relating them to the intensity of precipitation. They found as rain intensity increased so did the average raindrop size. Also they could use climato-logical rain rate data to infer drop sizes and effects on radar for different geographical locations and seasons of the year. Today our communications and weather reporting network is such that daily and hourly routine meteoro-logical observations are available on a global basis. After World War II the Stormy Weather Research Group at McGill University studied weather radar responses to rainfall. Marshall and Palmer (1948) then found that the raindrop size distribution relative to rain rate could be fitted by

$$N(D) = N_o \exp(-bD) \tag{37}$$

where N (D) is the number raindrop per unit volume (m^3) and per unit drop diameter D (mm), N_o is the limiting value of N (D) for D = 0 and is often taken as $N_o = 8000\ m^{-3}\ mm^{-1}$ and the coefficient b in units mm^{-1} is re-lated to the rainfall rate (R) in mm hr^{-1} by

$$b = 4.1\ R^{-0.21}\ mm^{-1} \tag{38}$$

Fig. 19 shows the raindrop size distribution as a function of rainfall rate, Laws and Parson data (broken line), and observations at Ottawa (dotted lines). It can be seen that good correspondence exists for all raindrop sizes and rainfall rates except for the smaller drops where the Marshall-Palmer method overpredicts the number of small raindrops. There is also an upper raindrop size limit because large drops (5 or 6 mm) become unstable and break up. Cole et al (1969) suggests limiting the Marshall-Palmer method to raindrop diameters between 0.75 and 2.25 mm for rain rates around 1 mm hr^{-1}, between 1.25 and 3 mm for rain rates near 5 mm hr^{-1}, and between 1.5 and 4.5 mm for rain rates greater than 25 mm hr^{-1}. In general, however, the Marshall-Palmer method performs reasonably well to provide an average drop size spectrum for a given rainrate. In Switzerland, Joss found the Marshall-Palmer model performed well for the same type of continuous precipitation in which it was developed but for drizzle and thunderstorm precipitation the coefficient N_o had to be increased and decreased by a factor of 4 and 1/8th, respectively.

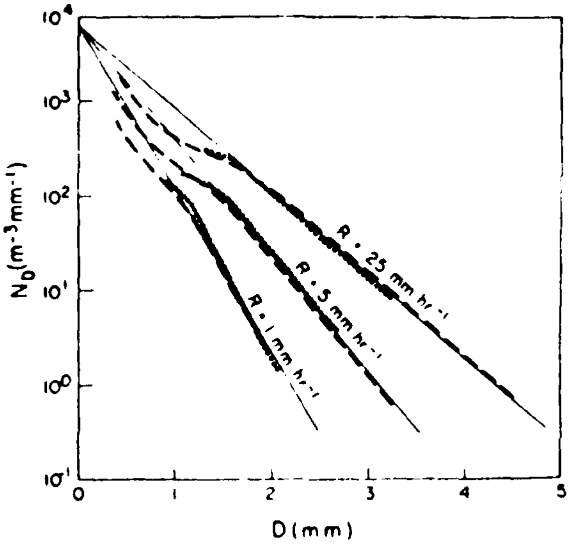

Fig. 19 Raindrop Size Distribution Vs. Rainfall Intensity

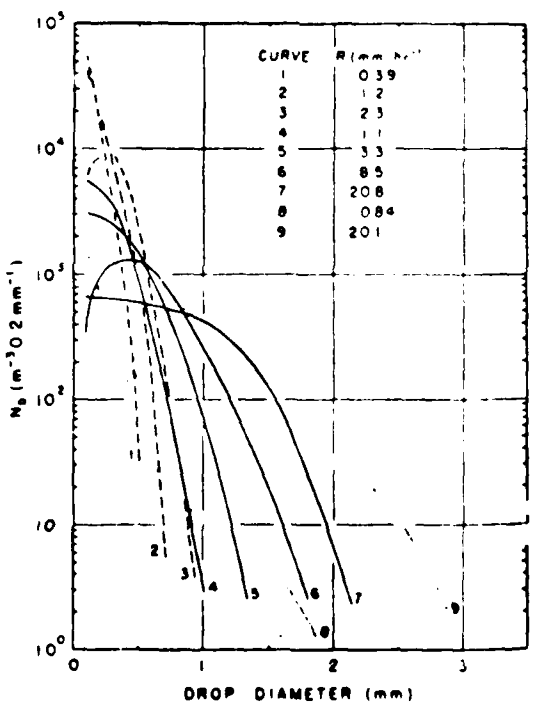

Fig. 20 Variety of Raindrop Size Distributions

Fig. 20 shows the large variety of raindrop size distributions that exist for different goegraphical locations, type of rain, and rainfall intensity. Blanchard's curves 1 - 3 are for Hawaiian in-cloud measurements made at or near the dissipating edge of non-freezing orographic clouds, while curves 4 - 7 represent data taken at the cloud base. Curves 8 - 9 are for non-orographic rain distributions. Curves 1 - 3 are typical of what is expected in a combined light rain, drizzle, and cloud environment, that is the particle size distribution is narrow and the peak frequency occurs at very small drop sizes. From the cloud base to the earth's surface it can be seen that the peak frequency or mode drop diameter increases and the distribution broadens as rainfall intensity increases. This is also observed in our particle size and number concentration distribution for mist, drizzle, light rain, moderate rain, and heavy rain in Tables 3, 4, 5, and 6, respectively.

TABLE 3 Mist and Drizzle Particles

PARTICLE SIZE AND NUMBER CONCENTRATION DISTRIBUTION

WEATHER TYPE	PARTICLE NUMBER DENSITY (Km^{-3})	PARTICLE RADIUS (Km)
MIST		
(0.05 mm/hr)	6×10^9	6.5×10^{-9}
	13×10^9	15×10^{-9}
	51×10^9	35×10^{-9}
	69×10^9	75×10^{-9}
	51×10^9	150×10^{-9}
	10×10^9	250×10^{-9}
	2×10^9	350×10^{-9}
	$.5 \times 10^9$	450×10^{-9}
	$.1 \times 10^9$	550×10^{-9}
DRIZZLE		
(.25 mm/hr)	6×10^9	6.5×10^{-9}
	13×10^9	15×10^{-9}
	51×10^9	35×10^{-9}
	80×10^9	75×10^{-9}
	85×10^9	150×10^{-9}
	26×10^9	250×10^{-9}
	9×10^9	350×10^{-9}
	3×10^9	450×10^{-9}
	1×10^9	550×10^{-9}
	$.3 \times 10^9$	650×10^{-9}
	$.1 \times 10^9$	750×10^{-9}

TABLE 4 Light Rain Particles

PARTICLE SIZE AND NUMBER CONCENTRATION DISTRIBUTION

WEATHER TYPE	PARTICLE NUMBER DENSITY (Km^{-3})	PARTICLE RADIUS (Km)
LIGHT RAIN		
(1 mm/hr)	6×10^{9}	6.5×10^{-9}
	13×10^{9}	15×10^{-9}
	51×10^{9}	35×10^{-9}
	85×10^{9}	75×10^{-9}
	106×10^{9}	150×10^{-9}
	54×10^{9}	250×10^{-9}
	24×10^{9}	350×10^{-9}
	11×10^{9}	450×10^{-9}
	5×10^{9}	550×10^{-9}
	2×10^{9}	650×10^{-9}
	1×10^{9}	750×10^{-9}
	$.4 \times 10^{9}$	850×10^{-9}
	$.2 \times 10^{9}$	950×10^{-9}
	$.3 \times 10^{9}$	1250×10^{-9}

TABLE 5 Moderate Rain Particles

PARTICLE SIZE AND NUMBER CONCENTRATION DISTRIBUTION

WEATHER TYPE	PARTICLE NUMBER DENSITY (Km^{-3})	PARTICLE RADIUS (Km)
MODERATE RAIN		
(4 mm/hr)	6×10^9	6.5×10^{-9}
	13×10^9	15×10^{-9}
	51×10^9	35×10^{-9}
	90×10^9	75×10^{-9}
	146×10^9	150×10^{-9}
	87×10^9	250×10^{-9}
	49×10^9	350×10^{-9}
	27×10^9	450×10^{-9}
	15×10^9	550×10^{-9}
	8×10^9	650×10^{-9}
	4×10^9	750×10^{-9}
	2×10^9	850×10^{-9}
	1×10^9	950×10^{-9}
	$.2 \times 10^9$	1250×10^{-9}
	$.1 \times 10^9$	1750×10^{-9}

TABLE 6 Heavy Rain Particles

PARTICLE SIZE AND NUMBER CONCENTRATION DISTRIBUTION

WEATHER TYPE	PARTICLE NUMBER DENSITY (Km^{-3})	PARTICLE RADIUS (Km)
HEAVY RAIN		
(16 mm/hr)	6×10^9	6.5×10^{-9}
	13×10^9	15×10^{-9}
	51×10^9	35×10^{-9}
	92×10^9	75×10^{-9}
	160×10^9	150×10^{-9}
	110×10^9	250×10^{-9}
	75×10^9	350×10^{-9}
	50×10^9	450×10^{-9}
	32×10^9	550×10^{-9}
	20×10^9	650×10^{-9}
	13×10^9	750×10^{-9}
	8×10^9	850×10^{-9}
	6×10^9	950×10^{-9}
	13×10^9	1250×10^{-9}
	2×10^9	1750×10^{-9}
	$.1 \times 10^9$	2250×10^{-9}

We have developed models to represent the simultaneous vertical variations in rain rate and liquid cloud content from the earth's surface to cloud top. Shown in Table 7 and 8 is our summer mid-latitude moderate (6 mm/hr) and heavy (15 mm/hr) rain model which provides air pressure, temperature, relative humidity, cloud content, and rain rate as a function of height in the atmosphere. Notice that they both have the same cloud base and top but differ significantly in cloud liquid water content and rain rate outside and within the cloud. The rain rate decreases rather slowly (at about 0.5 mm/hr/.25 km) from the surface to about midway through the cloud where it drops to near zero very rapidly. This same vertical variation in rain rate was found to also prevail at tropical latitudes for the same heavy rain situation, Fig. 9, but where the cloud top extends to far greater heights.

The general form of the exponential function, as given in our Eq. (4), has been simplified and used by Bent, Deirmendjian, and Khrgian and Mazin to specify static models of rain. If we take our Eq. (17) and insert the difference in velocity between the updraft (V_u) and terminal fall (V_T) velocity, (V_T - V_u), in the integrand it transposes the left hand side of the equation from the total mass concentration of liquid water into the rainfall rate. When the updraft is small relative to droplet terminal fall velocities then the equation simplifies, and, as shown in Fig. 21, remains

TABLE 7 Moderate Rain (6 mm/hr) For Summer Mid-Latitudes

RAIN MODEL ATMOSPHERE - MODERATE RAIN - 6 MM/HR 45 N MODEL - MID-LATITUDE

HEIGHT (KM)	PRESSURE (MB)	TEMPERATURE (DEG K)	RELATIVE HUMIDITY	CLOUD CONTENT (GM/CU M)	RAIN RATE (MM/HR)
0.000	1013.00	287.20	1.000	0.0000	6.000
.250	983.00	286.20	1.000	.2000	5.500
.500	954.00	285.10	1.000	.2800	4.400
.750	926.00	284.00	1.000	.3200	3.500
1.000	899.00	282.70	1.000	.3300	3.000
1.250	872.00	281.20	1.000	.3400	2.400
1.500	846.00	280.00	1.000	.3500	1.900
1.750	820.00	278.50	1.000	.3500	1.500
2.000	795.00	277.30	1.000	.3500	1.100
2.500	747.00	274.40	1.000	.3500	.600
3.000	701.00	271.20	1.000	.3500	.200
3.500	658.00	268.50	1.000	.3100	-0.000
4.000	616.00	265.00	1.000	.2500	-0.000
4.500	577.00	261.80	1.000	.1800	-0.000
5.000	540.00	258.00	1.000	.1300	-0.000
5.500	505.00	254.50	1.000	.0900	-0.000
6.000	472.00	251.50	1.000	.0500	-0.000
6.500	440.00	246.70	1.000	.0300	-0.000
7.000	410.00	242.20	1.000	.0100	-0.000
7.500	382.00	238.00	1.000	-0.0000	-0.000
8.000	356.00	234.50	1.000	-0.0000	-0.000
8.500	330.00	229.00	1.000	-0.0000	-0.000
9.000	307.00	225.00	.980	-0.0000	-0.000
9.500	285.00	220.00	.950	-0.0000	-0.000
10.000	264.00	223.20	.850	-0.0000	-0.000
11.000	226.00	216.70	.400	-0.0000	-0.000
12.000	193.00	216.70	.160	-0.0000	-0.000
13.000	165.00	216.70	.060	-0.0000	-0.000
14.000	141.00	216.70	.041	-0.0000	-0.000
15.000	120.00	216.70	.031	-0.0000	-0.000
16.000	103.00	216.70	.023	-0.0000	-0.000
17.000	87.90	216.70	.019	-0.0000	-0.000
18.000	75.00	216.70	.016	-0.0000	-0.000
19.000	64.10	216.70	.014	-0.0000	-0.000
20.000	54.70	216.70	.012	-0.0000	-0.000
22.000	40.00	218.70	.007	-0.0000	-0.000
24.000	29.	220.70	.004	-0.0000	-0.000
26.000	21.50	222.70	.002	-0.0000	-0.000
28.000	15.90	224.70	.001	-0.0000	-0.000
30.000	11.70	226.70	-0.000	-0.0000	-0.000
35.000	5.60	237.00	-0.000	-0.0000	-0.000
40.000	2.00	251.00	-0.000	-0.0000	-0.000
45.000	1.40	265.00	-0.000	-0.0000	-0.000
50.000	.80	270.70	-0.000	-0.0000	-0.000

TABLE 8   Heavy Rain (15 mm/hr) For Mid-Latitudes

RAIN MODEL ATMOSPHERE - HEAVY RAIN - 15 MM/HR   45 N MODEL - MID-LATITUDE

HEIGHT (KM)	PRESSURE (MB)	TEMPERATURE (DEG K)	RELATIVE HUMIDITY	CLOUD CONTENT (GM/CU M)	RAIN RATE (MM/HR)
0.000	1013.00	287.20	1.000	0.0000	15.000
.250	983.00	286.20	1.000	.3000	14.600
.500	954.00	285.10	1.000	.4000	14.300
.750	926.00	284.00	1.000	.4300	13.900
1.000	899.00	282.70	1.000	.4500	13.500
1.250	872.00	281.20	1.000	.4500	13.200
[illegible]	846.00	280.00	1.000	.4500	12.800
[illegible]	820.00	278.50	1.000	.4500	12.400
[illegible]	795.00	277.30	1.000	.4500	12.100
[illegible]	747.00	274.60	1.000	.4500	11.600
3.000	701.00	271.20	1.000	.4500	3.100
3.500	650.00	268.50	1.000	.4500	.010
4.000	616.00	265.00	1.000	.4500	-0.000
4.500	577.00	261.00	1.000	.3000	-0.000
5.000	540.00	258.00	1.000	.1700	-0.000
5.500	505.00	254.50	1.000	.1000	-0.000
6.000	472.00	251.50	1.000	.0500	-0.000
6.500	440.00	246.20	1.000	.0300	-0.000
7.000	410.00	242.20	1.000	.0100	-0.000
7.500	382.00	238.00	1.000	-0.0000	-0.000
8.000	356.00	234.50	1.000	-0.0000	-0.000
8.500	330.00	229.00	1.000	-0.0000	-0.000
9.000	307.00	225.00	.960	-0.0000	-0.000
9.500	284.00	220.00	[illegible]	-0.0000	-0.000
10.000	264.00	223.20	.650	-0.0000	-0.000
11.000	226.00	216.70	.490	-0.0000	-0.000
12.000	193.00	216.70	.150	-0.0000	-0.000
13.000	165.00	219.70	.060	-0.0000	-0.000
14.000	141.00	216.70	.041	-0.0000	-0.000
15.000	120.00	216.70	.031	-0.0000	-0.000
16.000	103.00	216.70	.023	-0.0000	-0.000
17.000	87.90	216.70	.019	-0.0000	-0.000
18.000	75.00	216.70	.016	-0.0000	-0.000
19.000	64.10	216.70	.014	-0.0000	-0.000
20.000	54.70	216.70	.012	-0.0000	-0.000
22.000	43.00	218.70	.007	-0.0000	-0.000
24.000	29.30	220.70	.004	-0.0000	-0.000
26.000	21.50	222.70	.002	-0.0000	-0.000
28.000	15.90	224.70	.001	-0.0000	-0.000
30.000	11.70	226.70	-0.000	-0.0000	-0.000
35.000	5.60	237.00	-0.000	-0.0000	-0.000
40.000	2.80	251.00	-0.000	-0.0000	0.000
45.000	1.40	265.00	-0.000	-0.0000	-0.000
50.000	.80	270.70	-0.000	-0.0000	-0.000

TABLE 9 Heavy Rain (15 mm/hr) For Tropical Latitudes

TROPICAL - 15 N HEAVY RAIN OF 15 MM/HR

HEIGHT (KM)	PRESSURE (MB)	TEMPERATURE (DEG K)	RELATIVE HUMIDITY	CLOUD CONTENT (GM/CU M)	RAIN RATE (MM/HR)
0.000	1013.00	298.00	.980	-0.0000	15.000
.250	985.00	297.20	1.000	.2000	14.500
.500	957.00	295.00	1.000	.3500	14.000
.750	930.00	294.00	1.000	.4000	13.500
1.000	904.00	293.80	1.000	.4500	13.000
1.250	878.00	293.10	1.000	.4500	12.600
1.500	853.00	292.60	1.000	.4500	12.200
1.750	828.00	291.40	1.000	.4500	11.900
2.000	804.00	289.50	1.000	.4500	11.600
2.500	750.00	287.10	1.000	.4500	11.000
3.000	714.00	285.10	1.000	.4500	10.500
3.500	672.00	282.00	1.000	.4500	10.200
4.000	632.00	280.60	1.000	.4500	9.900
4.500	594.00	278.00	1.000	.4500	9.700
5.000	558.00	275.40	1.000	.4500	9.500
5.500	524.00	273.00	1.000	.4500	5.500
6.000	491.00	270.20	1.000	.4500	.830
6.500	460.00	267.20	1.000	.4400	.200
7.000	431.00	264.30	1.000	.3600	.100
7.500	403.00	261.20	1.000	.3000	-0.000
8.000	376.00	257.00	1.000	.2500	-0.000
8.500	351.00	254.40	1.000	.1300	-0.000
9.000	328.00	251.00	1.000	.1400	-0.000
9.500	305.00	248.00	1.000	.0800	-0.000
10.000	285.00	242.90	1.000	.0300	-0.000
11.000	247.00	236.00	1.000	.0200	-0.000
12.000	211.00	235.60	1.000	.0100	-0.000
13.000	181.00	216.20	1.000	-0.0000	-0.000
14.000	154.00	206.30	1.000	-0.0000	-0.000
15.000	131.00	196.50	1.000	-0.0000	-0.000
16.000	110.00	192.60	.600	-0.0000	-0.000
17.000	92.30	194.00	.350	-0.0000	-0.000
18.000	77.60	198.00	.120	-0.0000	-0.000
19.000	65.20	202.00	.074	-0.0000	-0.000
20.000	55.40	206.70	.025	-0.0000	-0.000
22.000	40.10	214.60	.008	-0.0000	-0.000
24.000	29.30	219.20	.002	-0.0000	-0.000
26.000	21.50	223.60	.001	-0.0000	-0.000
28.000	16.90	227.90	-0.000	-0.0000	-0.000
30.000	11.60	232.40	-0.000	-0.0000	-0.000
35.000	5.04	245.00	-0.000	-0.0000	-0.000
40.000	2.99	258.50	-0.000	-0.0000	-0.000
45.000	1.50	269.00	-0.000	-0.0000	-0.000
50.000	.86	273.00	-0.000	-0.0000	-0.000

only dependent upon raindrop size. This rain rate equation could be used as a feedback mechanism and interate between it and the assumed form of the n(r) equation. That is to say, for the Marshall-Palmer equation one could assume an initial value for N_o, solve the integral to obtain a first guess value for R, compare the first R value with that observed, select a new value for N_o to reduce the difference between observed and computed R, and iterate to obtain the most applicable N_o for that rain. A similar approach can be used with the exponential or modified gamma function as an aid in modifying one of the parameters such as the shape factor and/or the coefficient A which is related to the liquid water content. Fig.22 shows the log log relation that exists between rainfall rate R (mm hr^{-1}) and liquid water content W_L (g m^{-3}) of raindrop. Two equations express this analytically as

$$W_L = 0.072 \ R^{.88} \qquad ([illegible])$$

for Marshall-Palmer rain and

$$W_L = 0.11 \ R^{.88} \qquad ([illegible])$$

for Joss drizzle.

In fact, for many obscuration problems it is possible to infer sensor attenuation directly by meteorological measurement of rainfall rate on liquid water content. This is especially noticeable in the microwave portion of the spectrum as shown in Fig. 23 as well as in the visible and infrared (Low 1979) for other weather features such as fog. Here, however, we are interested

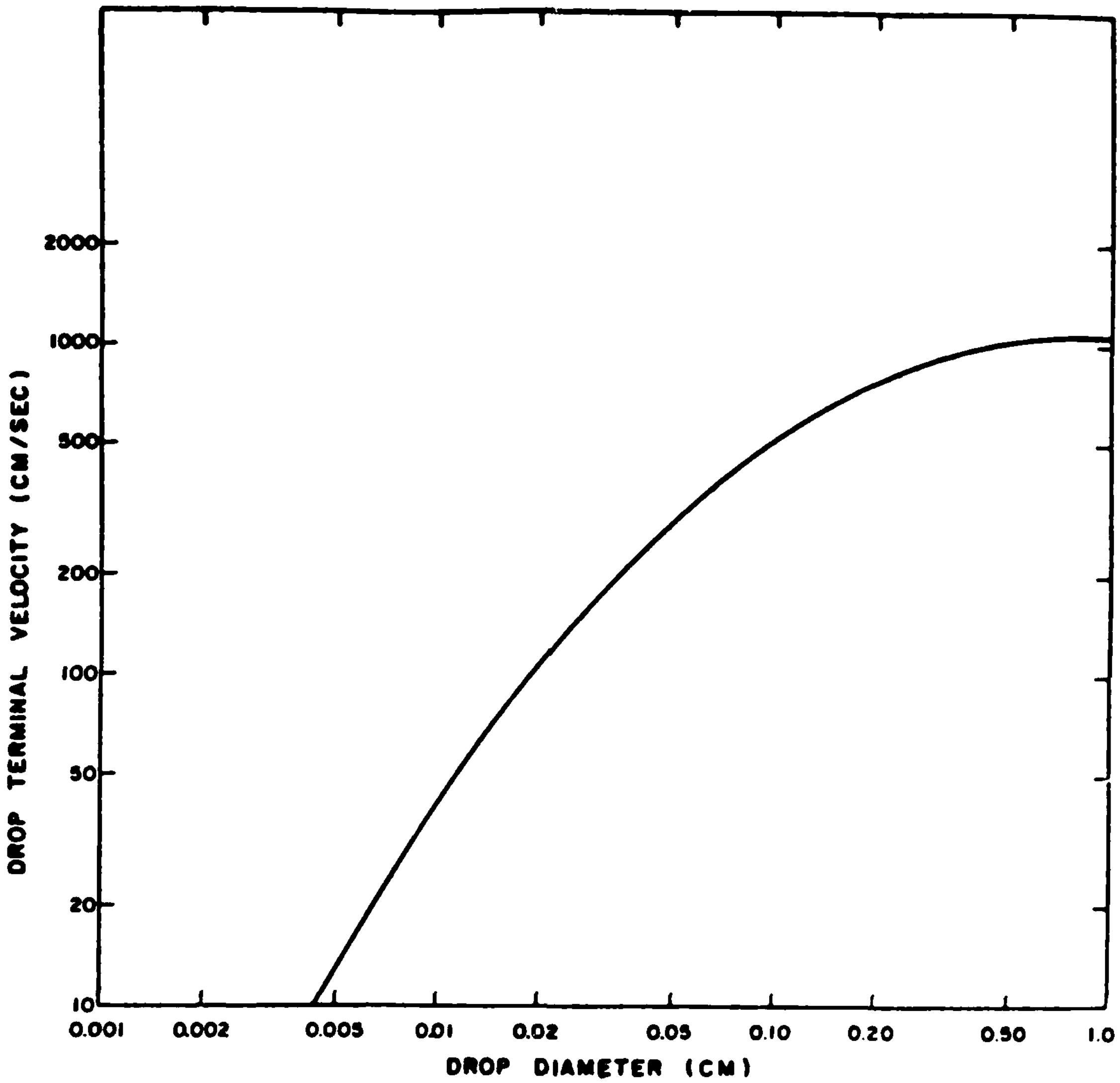

Fig. 21 Terminal Velocity Vs. Raindrop Size

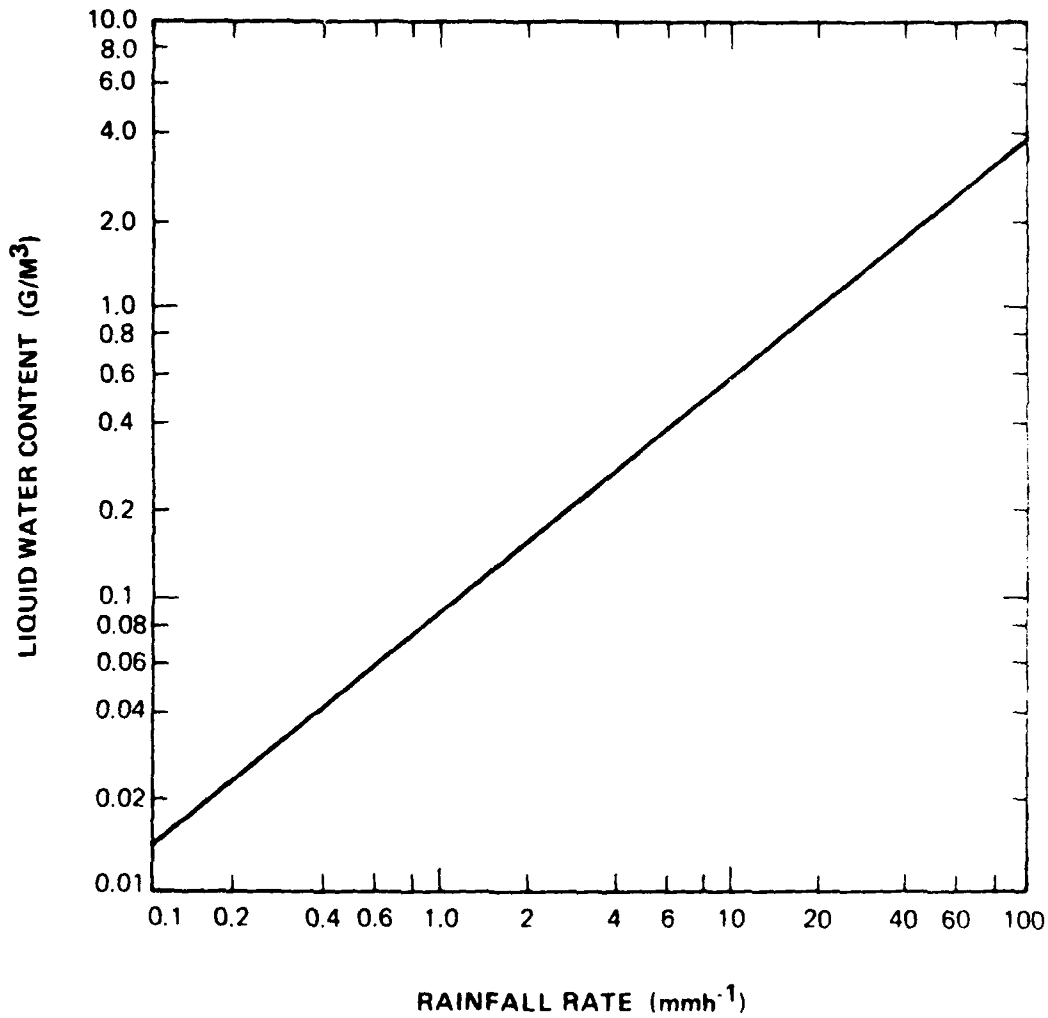

Fig. 22 **Liquid Water Content of Precipitation Versus Rainfall Rate**

in specification of raindrop size distributions and we have two strong candidates, the exponential approach that we previously used for fogs and clouds, and the Marshall-Palmer method. During the course of analyzing both approaches, we analyzed Marshall-Palmer type data from several sources, geographical locations, and rainfall types and was able to obtain a best fit equation that solves the coefficient N_o problem previously discussed. Figure 24 shows our plot of the variation of N_o coefficient relative to rainfall rate with best fit equation being

$$N_o = 12000 R^{-.72} \tag{41}$$

This equation alters the raindrop size distribution properly by increasing the population of small droplets in drizzle while decreasing the population of raindrops associated with showers and thunderstorms. By combining Equations (37), (38), and (41) it is now possible to have a single analytical expression for deriving raindrop particle size distributions for all rain/drizzle/mist type environments and geographical locations using only routinely measured rate of rainfall.

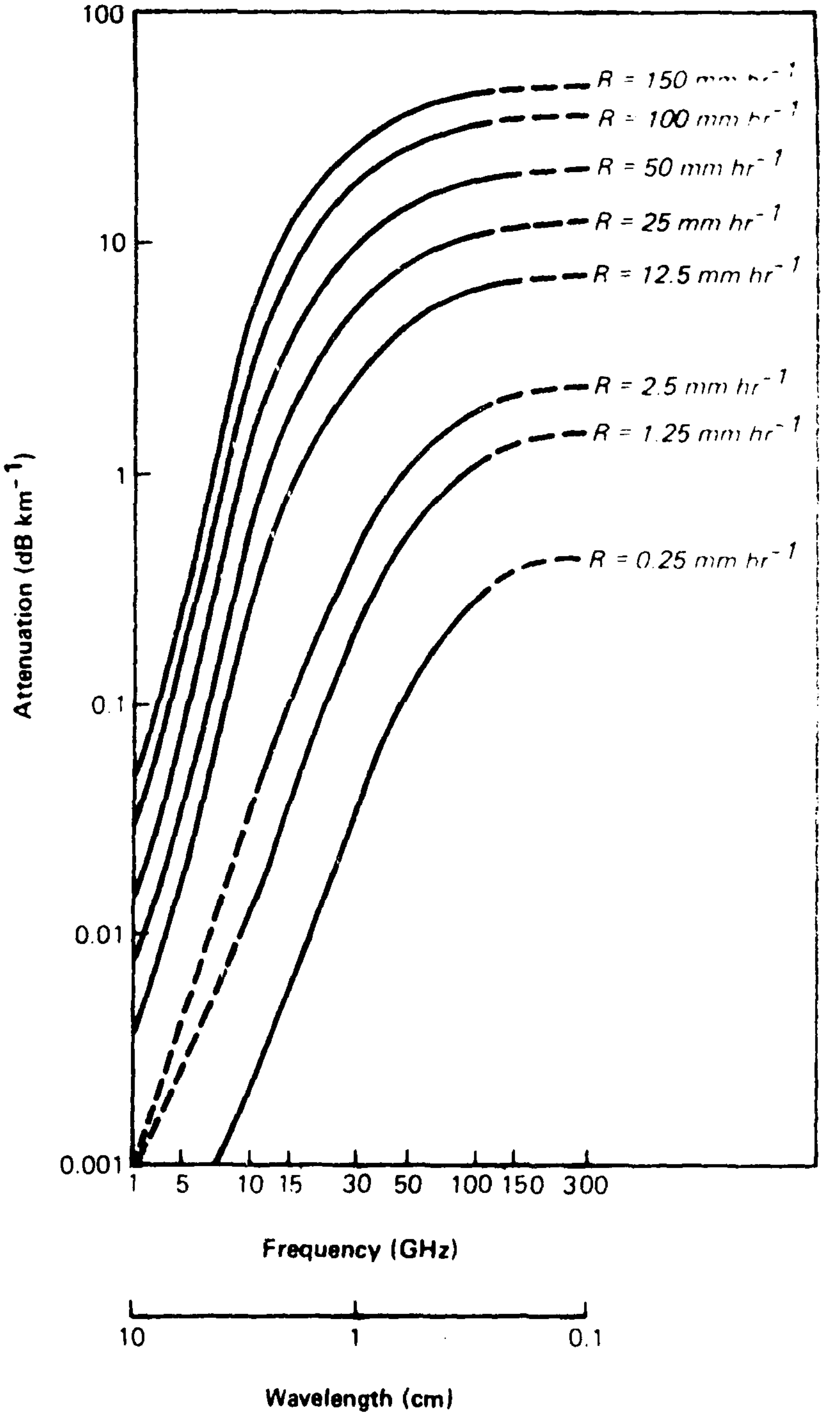

Fig. 23 **Attenuation vs. Frequency for Various Rainfall Rates**

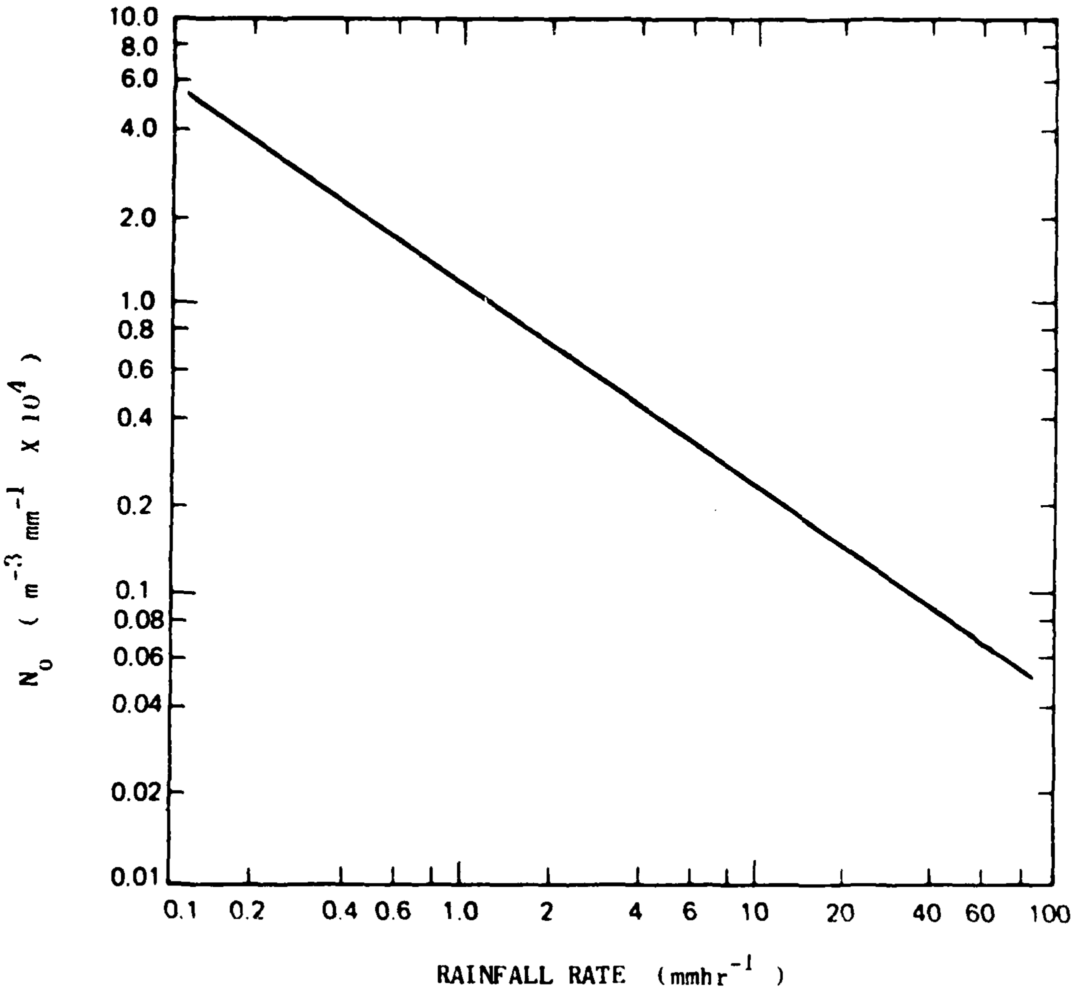

Fig. 24 Coefficient N_0 Versus Rainfall Rate

2.2.3.2 Dynamic Procedure

1. Using objective surface and upper air analysis techniques, such as CIVAS, obtain rainfall rate, height of cloud base and top, and horizontal changes in precipitation and cloud features.
2. Solve Equations (38) and (41) to obtain applicable values of [illegible] and N_O given the observed rainfall rate at the earth's surface.
3. Solve Eq. (37) to obtain raindrop size distributions over a selected range of raindrop diameters from 0.75 to 2.25 mm for rainrates equal to or less than 1 mm/hr, from 1.25 to 3 mm for rainrates greater than 1 mm/hr but less than 25 mm/hr, and from 1.5 to 4.5 mm for rainrates equal to or greater than 25 mm/hr.
4. Obtain the vertical distribution of rainfall rate by decreasing the surface value by 0.5 mm/hr per 0.25 km height in the atmosphere up to the mid-point height in the cloud at which the rainrate drops to zero.
5. Use the above derived rainrate distribution in the horizontal and vertical to derive changes in raindrop particle size distributions in the cloud-free air and cloud environment.

3. CONCLUSIONS AND RECOMMENDATIONS

1. Dynamic models are presented for specifying par le size distributions in horizontal and vertical directions for haze, fog, cloud and rain conditions given only routinely available meteorological data. Case studues showed these models performed well individually and when used together. This effort should be viewed as the first step in developing dynamic models that are responsive to observed and forecast weather changes. These models need to be applied, tested, modified, and improved.
2. More complete microphysical observations are needed not only to better understand atmospheric processes but also to provide better inputs to such meso- and synoptic scale models as developed here. Efforts should be made to incorporate and combine these dynamic models with such Army Cloud Fog Analysis System (CFAS) and Cloud/Ice/Visibility Analysis System (CIVAS) to depict natural obscurants at any desired time or location.
3. A more cooperative working environment must be created between the micro- and macro- atmospheric physicist. The micro-physicist feels threatened to think that Army users could be satisfied with only macro- scale data. In turn, the macro- physicist feels threatened when told only extensive microphysical observations

can provide necessary details. We have a lot to accomplish if we are to someday be in a position to help our Army provide day to day and hour by hour assessments of defensive and offensive weapon effectiveness. This requires all talents operating collectively with realistic guidelines on what meteorological data will be available for use in specifying and predicting obscuration for a Field Army.

AD-A107 637 GEO-ATMOSPHERICS CORP LINCOLN MA F/G 20/6
MODELS OF WEATHER ENVIRONMENTS ADVERSE TO ELECTRO-OPTICAL SYSTE--ETC(U)
SEP 81 W D MOUNT, B R FOW DAAD07-80-C-0047
UNCLASSIFIED ERADCOM/ASL-CR-81-0047-1 NL

2 OF 2
AD A
107637

END
DATE
FILMED
1 -82
DTIC

4 REFERENCES

Berry, E.W., and R.L. Reinhardt, "Modeling of Condensation and Collection Within Clouds," Phys. Sci., 16, (1973).

Blanchard, D.C., and Spencer, A.T., "Experiments on the Generation of Raindrop-Size Distributions by Drop Breakup," J. Atmos. Sci., 27, (1970).

Blifford, I.H., Jr., et al, "Particulate Models: Their Validity and Application," NCAR Technical Notes, Cat. No. NCAR-TN/PROC-68, Nat. Center for Atmos. Res., Boulder, CO, (1970).

Blifford, I.H., and Ringer, L.D., "The Size and Number Distribution of Aerosols in the Continental Troposphere," J. Atmos. Sci., 26,4(1969).

Blifford, I.H., Jr., "Tropospheric Aerosols," J. Geophys. Research, 75, 15, (1970).

Berry, E.X., "Cloud Droplet Growth by Collection," J. Atmos. Sci. 24, 6, (1967).

Best, A.C. "The Size Distribution of Raindrops," Q.J.R.M.S., 76, (1950).

Bigg, E.K., "Comparison of Aerosol at Four Baseline Atmospheric Monitoring Stations," J. Appl. Meteorol., 19, (1980).

Bigg, E.K., "Some Properties of the Aerosol at Mauna Loa Observatory," J. Appl. Meteorol., 16, (1977).

Brown, R. and Roach W.T. "The physics of Radiation Fog: II - A Numerical Study," Q.J.R.M.S., 102, 432, p. 355, (1976).

Brown, R., "A Numerical Study of Radiation Fog with an Explicit Formulation of the Microphysics," Q.J.R.M.S., 106, 450, (1980).

Carbone, R.E. and Nelson, L.D., "The Evolution of Raindrop Spectra in Warm-Based Convective Storms as Observed and Numerically Modeled," JAS, 35, (1978).

Carrier, L.W. et al. "The Backscattering and extinction of Visible and Infrared Radiation by Selected Major Cloud Models," Appl. Opt., 6, (1967).

Carswell, A.I., "Laser Measurements in Clouds," IFAORS Abstract Digest, Clouds: Their Formation, Optical Properties and Effects, (1980).

Chagnon, C.W., and Junge, C.E., "The Vertical Distribution of Sub-Micron Particles in the Stratosphere," Handbook of Geophysics and Space Environments, J. Meteorol. 18, p. 746, (1961).

Chappell, C.F., and Smith, D.R., "Simulation of Cold Cloud Precipitation in a Three-dimentional Mesoscale Model," NOAA Tech. Rept., ERL-381-APCL-40, 26 pp., (1976).

Chen, C.C., "Attenuation of Electromagnetic Radiation by Haze, Fog, Clouds and Rain," USAF Project Rand, R-1964-PR, Santa Monica, CA., (1975).

Christian, H., Holmes, C.R., Bullock, J.W., Gaskell, W., Illingsworth, A.J., and Latham, J., "Airborne and Ground-Based Studies of Thunderstorms in the Vicinity of Langmuir Laboratory," Q.J.R.M.S., 106, (1980).

Clark, W.E., and Whitby, K.T., "Concentration and Size Distribution Measurments of Atmospheric Aerosols and a Test of the Theory of Self-Preserving Size Distributions," J. Atmos. Sci., 24, (1967).

Cohen, I.D., Capt, USAF, "Marine Boundary Layer Sampling : Flight No. 2," AF Geoph. Lab., AFGL-TR-79-0242, Res. Papers, 678, (1979).

Cole, A.E., Donaldson, R.J., Dyer, R., Kantor, A.J., Skrivanek, "Precipitation and Clouds: A Revision of Chapter 5, Handbook of Geophysics and Space Environments," USAF Off. of Aerospace Res., AFCRL-69-0487, (1969).

Cooper, W.A., and Saunders, C.P.R., "Winter Storms over the San Juan Mountains, Part II: Microphysical Processes," J. Appl. Meteor., 19, (1980).

Corradini, C., and Tonna, G., "The Parameterization of the Gravitational Water Flux in Fog Models," J. Atmos. Sci., 37, (1980).

Cotton, W.R., "Cloud Physics: A Review for 1975-1978 IUGG Quadrennial Report," Reviws of Geophysics and Space Physics, 17, 7, (1979).

Cress, T.S., "Altitudinal Variations of Aerosol Size Distributions Over Northern Europe," AF Geophys. Lab. Report, Hanscom AFB, MA, (1979). (since published as AFGL-TR-80-0178)

Deirmendjian, D., "Complete Microwave Scattering and Extinction Properties of Polydispersed Cloud and Rain Elements," USAF Project Rand Report, R-422-PR, (1963).

Delany, A.C., Pollock, W.H., and Shedlovsky, J.P., "Tropospheric Aerosol: The Relative Contribution of Marine and Continental Components," J. Geophys. Res., 78, 27, p. 6249-6265, (1973).

Donnadieu, G., "Comparison of Results Obtained with the VIDIAZ Spectro-Pluviometer and the Joss-Valdvogel Rainfall Disdrometer in a "Rain of a Thundery Type"," J. Appl. Meteor., 19, (1980).

Downs, A.R., "A Review of Atmospheric Transmission Information in the Optical and Microwave Spectral Regions," USA Ballistic Res. Labs, Aberdeen Proving Ground, MD, AD/A-035 059, (1976).

East, T.W.R., "An Inherent Precipitation Mechanism in Cumulus Clouds," Q.J.R.M.S., 83, (1957).

Eldridge, R.G., "Haze and Fog Aerosol Distributions," J. Atmos. Sci., 23, (1966).

Elterman, L., "Parameters for Attenuation in the Atmospheric Windows for Fifteen Wavelengths," Appl. Opt., 3, 745-749, (1964).

Elterman, L., "UV, Visible and IR Attenuation for Altitudes to 50 Km, 1968," AF CRL-68-0153.

Elterman, L., "Vertical-Attenuation Model With Eight Surface Meteorological Ranges 2 to 13 Kilometers," Hanscom AFB Report, (1970).

Falcone, V.J.,Jr., Abreu, L.W., and Shettle, E.P., "Atmospheric Attenuation of Millimeter and Submillimeter Waves: Models and Computer Code," Hanscom AFB, MA, Report, AFGL-TR-79-0253, Optical Phys. Div., Proj. 7670, (1979).

Federer, B., and Waldvogel, A., "Hail and Raindrop Size Distributions from a Swiss Multicell Storm," J. Appl. Meteor., 14, p. 91-97, (1975).

Fenn, R.W., and Shettle, E.P., "Optical Aerosol Models and Light Scattering Programs," AF Geophys. Lab., Hanscom AFB, MA.

Fenn, R.W., Gerber, W.E., and Wasshausen, E., "Measurements of the Sulfate and Ammonium Components of the Artic Aerosol of the Greenland Ice Cap," Handbook of Geophysics and Space Environments, (1963).

Fitzgerald, J.W., "Approximation Formulas for The Equilibrium Size of an Aerosol Particle as a Function of Its Dry Size and Composition and the Ambient Relative Humidity," J. Appl. Meteor., 14, (1975).

Fitzgerald, J.W., "Angular Truncation Error of the Integrating Nephelometer in the Fog Droplet Size Range," J. Appl. Meteor., 16, (1977).

Fletcher, N.H., The Physics of Rainclouds, Cambridge University Press, London, pp. 112-121, 267-268, (1966).

Fujiwara, M., "Raindrop-Size Distribution from Individual Storms," J. Atmos. Sci., 22, (1965).

Garland, J.A., "Some Fog Droplet Size Distributions Obtained by an Impaction Method," Q.J.R.M.S., 97, pp. 483-494, (1971).

Gerber, H.E., "A Saturation Hygrometer for the Measurement of Relative Humidity Between 95 and 105%," J. Appl. Meteor., 19, (1980).

Gillespie, J.R., and List, R., "Evolution of Raindrop Size Distributions in Steady State Rainshafts," Dept. of Phys., Univ. of Toronto, (1976).

Griggs, M. and Marggraf, W.A., "Measurment of Cloud Reflectance Properties and the Atmospheric Attenuation of Solar and Infrared Energy," Office of Aerospace Res., Bedford, MA, Contract No. AF19(628)-5517, (1967).

Hamilton, P.M., "Vertical Profiles of Total Precipitations in Shower Situations," Q.J.R.M.S., 92, (1966).

Hanel, G., "The Single-Scattering Albedo of Atmospheric Aerosol Particles as a Function of Relative Humidity," J. Atmos. Sci., 33, (1976).

Herzegh, P.H., and Hobbs, P.V., "The Mesoscale and Microscale Structure and Organization of Clouds and Precipitation in Midlatitude Cyclones. II: Warm-Frontal Clouds," J. Atmos. Sci., 37, 3, (1980).

Hildebrand, P.H., "Iterative Correction for Attenuation of 5 cm Radar in Rain," J. Appl. Meteor., 17, (1978).

Hobbs, P.V., Politovich, M.K., and Radke, L.F., "The Structures of Summer Convective Clouds in Eastern Montana. I: Natural Clouds," J. Appl. Meteor., 19, (1980).

Hobbs, P.V., Matejka, T.J., Herzegh, P.H., Locatelli, J.D., and Houze, R.A., Jr., " The Mesoscale and Microscale Structure and Organization of Clouds and Precipitation in Midlatitude Cyclones. I: A Case Study of a Cold Front," J. Atmos. Sci., 37, 3, (1980).

Hobbs, P.V., "Scales Involved in the Formation and Organization of Clouds and Precipitation," IFAORS Abstract Digest, Clouds: Their Formation, Optical Properties and Effects, (1980).

Hofmann, D.J. et al., "Stratospheric Aerosol Measurements IV: Global Time Variations of the Aerosol Burden and Source Considerations," J. Atmos. Sci., 33, 9, p. 1782-1788. (1976).

Hofmann, D.J. and Rosen, J.M., "Balloon Observations of the Time Development of the Stratospheric Aerosol Event of 1974-1975," J. Geophys. Res., 82, 9, p. 1435-1440, (1977).

Houze, R.A., Hobbs, P.V., Herzegh, P.H., and Parsons, D.B., "Size Distribution of Precipitation Particles in Frontal Clouds," J. Atmos. Sci., 36, (1979).

Howell, W.E., "The Growth of Cloud Drops in Uniformly Cooled Air," J. Meteor., 6, (1949).

Hudson, J.G., and Squires, P., "Microphysics of Post Ana Fogs," International Conference on Cloud Physics, Boulder Colorado, (1976).

Hudson, J.G., "Relationship Between Fog Condensation Nuclei and Fog Microstructure," J. Atmos. Sci., 37, (1980).

Huffaker, R.M., et al., "Feasibility Study of Sattelite-Borne Lidar Global Wind Monitoring System," NOAA Technical Memorandum ERL WPL-37, (1978).

Hunt, G., "Diurnal Properties Of Clouds From Geostationary Satellite Observations," IFAORS Abstract Digest, Clouds: Their Formation, Optical Properties and Effects, (1980).

Jones, D.M.A., "Rainfall Drop Size Distribution and Radar Reflectivity," Meteor. Lab. Res. Rep. No. 6, Illinois State Water Survey (NTIS No. AD101799.), (1956).

Johnson, D.B., "The Influence of Cloud-Base Temperature and Pressure on Droplet Concentration," J. Atmos. Sci. 37, (1980).

Joss, J., and Waldvogel, A., "Raindrop Size Distribution and Sampling Size Errors," J. Atmos. Sci., 26, (1969).

Joss, J., and Gori, E.G., "Shapes of Raindrop Size Distributions," J. Appl. Meteor., 17, (1978).

Jones, M.A., and Sims, A.L., "Climatology of Instantaneous Rainfall Rates," J. Atmos. Sci., 17, (1978).

Jiusto, J.E., "Considerations in the Optical Characterization of the Atmosphere," Atmos. Sci. Lab., White Sands Missile Range, NM, ASL-CR-79-0100-3, (1979).

Junge, C.E., "Vertical Profiles of Condensation Nuclei in the Stratosphere," Handbook of Geophysics and Space Environments, J. Meteor., 18, p. 501, (1961).

Kampe, H.J.A., and Weikmann, H.K., "Physics of Clouds," Meteor. Monographs, 3, 18, (1957).

Kaveney, W.J., Feddes, R.G., and Liou, K-N, "Statistical Inference of Cloud Thickness from NOAA 4 Scanning Radiometer Data," Monthly Weather Review, 105, pp. 99-107, (1977).

Kessler, R., "Kinimatical relations between Wind and Precipitation Distributions II," J. Meteor., 18, (1961).

Kessler, E., "On the Distribution and continuity of water substance in Atmospheric Circulations," Meteor. Monogr., 10, 84pp., (1969).

Kessler, E., "Model of Precipitation and Vertical Air Current," Tellus, XXVI, pp. 519-542, (1974).

Kennedy, J.S., and Norberg, W., "Circulation Features of the Stratosphere Derived from Radiometric Temperature Measurements with the TIROS VII Satellite," J. Atmos. Sci., 24, 6, (1967).

Kessler, E., III, and Atlas, D., "Model Precipitation Distributions," Aero/Space Eng., Dec., (1959).

Khrgian, A.K. and Mazin, I.P., "Analysis of Methods of Characterizing Raindrop Distribution Spectra," Tr. Tsents. Aerolog. Observ. Moscow, (translation) 17, 36-46, (1956).

King, M.D., and Herman, B.M., "Determination of the Ground Albedo and the Index of Absorption of Atmospheric Particulates by Remote Sensing. Part II: Theory," J. Atmos. Sci.,36, (1979).

Kneizys, F.X., Shettle, E.P., Gallery, W.O., Chetwynd, J.H., Jr., Abreu, L.W., Selby, J.E.A., Fenn, R.W., and McClatchley, R.A., "Atmospheric Transmittance/Radiance: Computer Code LOWTRAN 5," Optical Physics Division, Hanscom AFB, AFGL-TR-80-0067, (1980).

Knollenberg, R.G., "Techniques for Probing Cloud Structures," IFAORS Abstract Digest, Clouds: Their Formation, Optical Properties and Effects, (1980).

Kocmond, W.C., Pilie, R.J., Eadie, W.J. and Mack,E.J., "Recent Fog Modification Research at Cornell Aeronautical Laboratory," Second National Conference on Weather Modification, Santa Barbara, (1970).

Kreitzberg, C.W., and Rasmussen, R.G., "Treatment of Cloudiness in Regional Scale Numerical Weather Prediction Models," Preprint Volume, Conf. on Cloud Physics and Atmos. Electricity, Issaquah, WA, Amer. Meteor. Soc., 506-513, (1978).

Kreitzberg, C.W., Mount, W.D., and Fow, B.R., "Preliminary Evaluation of Meteorological Models for Moisture Depiction and Prediction for Electro-Optical Applications," Final Report for Atmos. Sci. Lab., White Sands Missile Range, NM, Contract DAAG29-76-D-0100 , (1979).

Krishnamurti, T.N., Ramanathan, H-L P., Pasch R.J., Molinari, J., "Cumulus Parameterization and Rainfall Rates I," Monthly Weather Review, 108, (1980).

Kumai, M., "Arctic Fog Droplet Size Distribution and Its Effect on Light Attenuation," J. Atmos. Sci., 30, (1973).

Kunkel, B.A., "Fog Drop-Size Distributions Measured with a Laser Hologram Camera," J. Appl. Meteor., 10, (1971).

Lala, G.G., Mandel, E., and Jiusto, J.E., "A Numerical Evaluation of Radiation Fog," J. Atmos. Sci., 32, 720-728, (1975).

Langille, R.C., and Gunn, K.L.S., "Quantitative Analysis of Vertical Structure in Precipitation," J. Meteor., 5, (1948).

LaRocca, A.J., and Turner, R.E., "Atmospheric Transmittance and Radiance: Methods of Calculation," Contract Nos. N00014-73-A-0321-0002 and N00014-74-C-0285, Research Ins. of MI, Ann Arbor, (1975).

Laws, J.O., and Parsons, D.A., "The Relation of Raindrop-size to Intensity," Transactions, American Geophysical Union, 24, Pt. 2, (1943).

Lee, I.Y., Hanel, G., and Pruppacher, H.R., "A Numerical Determination of the Evolution of Cloud Drop Spectra due to Condensation on Natural Aerosol Particles," J Atmos. Sci., 37, (1980).

Lewis, R.E., "Meteorological aspects of Aircraft Icing," Compendium of Meteor. T. F. Malone, ed. AMS, Boston, (1951).

Lowe, P.R., "An Approximating Polynomial for Computation of Saturation Vapor Pressure," J. Appl. Meteor., 16, p. 100-103, (1977).

Low, D.H.R., "A Theoretical Investigation of Cloud/Fog Extinction Coefficients and Their Spectral Correlations," Atmos. Phys., 52, 1, (1979).

Low, R.D.H., "Fog Evolution in the Visible and Infrared Spectral Regions and Its Meaning in Optical Modeling," Atmospheric Sciences Laboratory, White Sands Missle Range, NM, (1979).

Lovejoy, S., and Austin, G.L., "The Estimation of Rain from Satellite-Borne Microwave Radiometers," Q.J.R.M.S., 106, pp. 255-276, (1980).

MacDonald, J.E., "The Saturation Adjustment in Numerical Modeling of Fog," J. Atmos. Sci., 20, pp. 476-478, (1963).

Malm, W.C., Walther, E.G., and Cudney, R.A., "The Effects of Water Vapor, Ozone and Aerosol on Atmospheric Turbidity," J. Appl. Meteor., 16, (1977).

Matejka, T.J., Houze, R.A., Jr., and Hobbs, P.V., "Microphysics and Dynamics of Clouds associated with Mesoscale Rainbands in Extratropical Cyclones," Q.J.R.M.S., 106, pp. 29-56, (1980).

Mathai, C.V., Harrison, A.W., and Mathews, T., "Aerosol Particle Size Distribution (0.1 - 1.0 m) During the Chinooks of 1979 over Calgary, Canada," J. Appl. Meteor., 19, (1980).

Marshall, J.S., and Palmer, W.M., "The Distribution of Raindrops with Size," J. Meteor., 5, pp. 165-166, (1948).

Mason, B.J., D.Sc., F.R.S., "The Physics Of Clouds," Clarendon Press, Oxford, Second Edition, (1971)., 671 pp.

McCartney, E.J., "Optics of the Atmosphere,"John Wiley & Sons, New York, 407 pp.

McClatchey, R.A., and Selby, J.E.A., "Atmospheric Attenuation of Laser Radiation From 0.76 to 31.25 m," Optical Physics Lab. Hanscom AFB, AFCRL-TR-74-0003, (1974).

McClatchley, R.A., Fenn, R.W., Selby, J.E.A., Volz, F.E.,and Garing, J.S., "Optical Properties of the Atmosphere" (Third Edition), AF CRL-72-0497, 1972.

Medhurst, R.G., "Rainfall Attenuation of Centimeter Waves: Comparison of Thoery and Measurement," Tefe Transactions on antennas and Propagation, ed. Falcone, pp. 550-556, (1955).

Meyer, M.B., Jiusto, J.E., and Lala, G.G., "Measurements of Visual Range and Radiation-Fog (Haze) Microphysics," J. Atmos. Sci., 37, pp. 622-629, (1980).

Monohan, H.H., "A Summary of Meteorological Data Sources in the United States and Studies Relating to the Climatology of Central Europe," ASL Internal Report, (1979).

Monohan, H. H., and Cionco, R.M., "An interperative Review of Existing Capabilities for Measuring and Forecasting Selected Weather Variables (Emphasizing Remote Means), ASL Report, ASL-TR-0001, (1978).

Mooradian, G.C., and Geller, M., "Pulsed Blue-Green Propagation Through Clouds and Fogs", IFAORS Abstract Digest, Clouds: Their Formation, Optical Properties and Effects, (1980).

Mount, W.D., and Fow, B.R., "Millimeter and microwave obscuration for 10 mm to 10 cm Wavelengths. Final Rept. GAC-78-003 to Battelle Columbus Laboratories. (1978).

Mount, W.D., Fow, B.R., and Mount, B.D., "Cloud/Icing/Visibility Analysis System (CIVAS) and Forecast Development Plan," Final Rept. GAC-79-03-05-02 to White Sands Missile Range. (1980).

Mount, W.D., Fow, B.R., Mount, B.D., and Rapp, J.O., "Sensitivity Study of CFAS and CFAR Objective Analysis Techniques," Final Rept. GAC-78-CR-002 to White Sands Missile Range. (1978).

Mueller, E.A. and Jones, D.M.A., "Dropsize distributions in Florida," Preprints 8th Weather Radar Conf., San Francisco, Amer. Meteor. Soc., 299-305. (1960).

Norton, C.C., Mosher, F.R., Hinton, B., Martin, D.W., Santek, D., and Kuhlow, W., "A Model for Calculating Desert Aerosol Turbidity over the Oceans from Geostationary Satellite Data," J. Appl. Meteor., 19, 6, (1980).

Ohtake, T., "Observations of Size Distributions of Hydrometers Through the Melting Layer," J. Atmos. Sci., 26, (1969).

Pasceri, R.E., and Friedlander, S.K., "Measurements of the Particle Size Distribution of the Atmospheric Aerosol: II. Experimental Results and Discussion, " J. Atmos. Sci., 22, (1965).

Patterson, E.M., Kiang, C.S., Delany, A.C., Wartburg, A.F., Leslie, A.C.D., and Huebert, B.J., "Global Measurement of Aerosols in Remote Continental and Marine Regions: Concentrations, Size Distributions, and Optical Properties," (paper 80C1078), J. Goephys. Res. 85, C12, (1980).

Pasqualucci, F., "Drop-Size Distributions in Unicell, Multicell, and Squall Line Storms," Nat. Conf. on Cloud Physics, 6.2.8, Boulder, Colo., (1976).

Passarelli, R.E.JJr., "Notes and Correspondence: Comments on "Size Distributions of Precipitation Particles in Frontal Clouds," J. Atmos. Sci., 37, (1980).

Patterson, E.M., and Gillette, D.A., "Measurements of Visibility VS Mass-Concentration for Airborne Soil Particles," Atmos. Environment, 11, pp. 193-196, Pergamon Press, (1977).

Patterson, E.M., and Gillette, D.A., "Commonalities in Measured Size Distributions for Aerosols Having a Soil-Derived Component," J. Geophys. Sci., 82, 15, (1977).

Pilie, R.J., Mack, E.J., Kocmond, W.C., Eadie, W.J., and Rogers, C.W., "The Life Cycle of Valley Fog. Part II: Fog Microphysics," J. Appl. Meteor., 14, (1975).

Pilie, R.J., Mack, E.J., Kocmond, W.C., Rogers, C.W., and Eadie, W.J., "The Life Cycle of Valley Fog. Part I: Micrometeorological Characteristics," J. Appl. Meteor., 14, (1975).

Pinnick, R.G., Hoihjelle, D.L., Fernandez, G., Stenmark, E.B., Lindberg, J.D., Hoidale, G.B., and Jennings, S.G., "Vertical Structure in Atmospheric Fog and Haze and Its Effects on Visible and Infrared Extinction," J. Atmos. Sci., 35, (1978).

Platt, C.M.R., "Transmission of Submillimeter Waves Through Water Clouds and Fogs," J. Atmos. Sci., 27, (1970).

Pratte, F.J., Huffaker, R.M., Lawrence, T.R., and Loveland, R., "System Considerations of a Long Range Coherent Lidar Wind Sensor With Particular Emphasis on Real Weather Effects," NOAA Tech. Memo. ERL WPL-42, Wave Propagation Laboratory, Boulder Colorado, (1979).

Prospero, J.M., and Carlson, T.N., "Vertical and Aerosol Distribution of Saharan Dust Over the Western Equatorial North Atlantic Ocean," J. Geophys. Res., 77, p. 5255-5265, (1972).

Pruppacher, H.R., "The Microstructure of Atmospheric Clouds and Precipitation," IFAORS Abstract Digest, Clouds: Their Formation, Optical Properties and Effects, (1980).

Pruppacher, H.R., and Klett, J.D., "Microphysics of Clouds and Precipitation," p. 9-27, (1980).

Pueschel, R.F., and Kuhn, P.M., "Infrared Absorption of Tropospheric Aerosols: Urban and Rural Aerosols of Phoenix, Arizona," J. Geophys. Res., 80, 21, (1975).

Quenzel, H., "Determination of Size Distribution of Atmospheric Aerosol Particles from Spectral Solar Radiation Measurements," J. Geophys. Res., 75, 15, (1970).

Radke, L.F., Hobbs, P.V., and Eltgroth, M.W., "Scavenging of Aerosol Particles by Precipitation," J. Appl. Meteor. 19, (1980).

Reitan, C.H., "Droplet Size Measurements in Convective Clouds," In Artificial Stimulation of Rain, (eds. H. Weickmann and W. Smith), p. 1-4, Pergamon Press, NY, (1957).

Roach, W.T., Brown, R., Caughey, S.J., Garland, J.A., and Readings, C.J., "The Physics of Radiation Fog: I - A Field Study," Q.J.R.M.S., 102, 432, (1976).

Roach, W.T., "On the Effect of Radiative Exchange on the Growth by Condensation of a Cloud or Fog Droplet," Q.J.R.M.S., 102, 432, (1976).

Rogers, R.R., "A Short Course in Cloud Physics," 2nd Edition, 235 pp., Pergamon Press, NY, (1979)

Ryan, B.F., "A Model to Derive Precipitation Patterns and Vertical Velocities in Large-Scale Rain Systems," Q.J.R.M.S., 106, pp. 201-212, (1980).

Savage, R.C., "The Radiative Properties of Hydrometers at Microwave Frequencies," J. Appl. Meteor., 17, p. 904-907, (1978).

Selby, J.E.A., Shettle, E.P., and McClatchey, R.A., "Atmospheric Transmittance From 0.25 to 28.5 m: Supplement LOWTRAN 3B (1976)," AFGL-TR-76-0258 Environmental Research Papers, Hanscom AFB, (1976).

Shettle, E.P., and Fenn, R.W., "Models for the Aerosols of the Lower Atmosphere and the Effects of Humidity Variations on Their Optical Properties," AFGL-TR-79-0214 Env. Res. Papers No. 676, Air Force Geophysics Laboratory. (1979).

Shettle, E.P., "Comment on Atmospheric Aerosol Size Spectra: Rapid Concentration Fluctuations and Bimodality" by T.E. Graedel and J.P. Franey," J. Geophys. Res., 80, 21, (1975).

Silverman, B.A., and Sprague, E.D., "Airborne Measurement of In-Cloud Visibility," p. 271-276, Second National Conference on Weather Modification, Santa Barbara, (1970).

Silverman, B.A., "An Eulerian Model of Warm Fog Modification," Air Force Cambridge Res. Labs., Bedford, MA.

Smith, P.L., Myers, C.G., and Orville, H.D., "Radar Reflectivity Factor Calculations in Numerical Cloud Models Using Bulk Parameterization of Precipitation,"J. Appl. Meteor. 14, (1975).

Spilhaus, A.F., "Drop Size, Intensity, and Radar Echo of Rain," J. Met., 5, 161, (1948).

Srivastava, R.C., "Size Distribution of Raindrops Generated By Their Breakup and Coalescence," J. Atmos. Sci., 28, p. 401-415, (1971).

Srivastava, R.C., "Parameterization of Raindrop Size Distributions," J. Atmos. Sci., 35, 108-117, (1978).

Srivastava, R.C., and Atlas, D., "Growth, Motion and Concentration of Precipitation Particles in Convective Storms," J. Atmos. Sci., 26, (1969).

Steinvall, O., "Computed Mie Scattering Properties for Laser Wavelengths in Various Atmospheric Media," FCA-2-C-2662-B1-B3, Res. Inst. of Nat. Def. 41 p.,(1971).

Tag, P.M., Johnson, D.B., ENS, Hindman, E.E. II, "Engineering Fog-Modification Experiments by Computer Modelling," Second National Conf. on Weather Modification, Santa Barbara, (1970).

Toon, O.B., and Pollock, J.B., "A Global Average Model of Atmospheric Aerosols for Radiative Transfer Calculations," J. Appl. Meteor., 15, [illegible], p. 225-246, (1976).

Trusty, G.L., and Cosden, T.H., "An Aerosol Measurement System For Laser/Aerosol Interaction Studies," Proceedings of the Optical-Submillimeter Atmospheric Propagation Conference, Vol. 1, (1976).

Twomey, S., and Warner, J., "Comparison of Measurements of Cloud Droplets and Cloud Nuclei," J. Atmos. Sci., p. 402-403, 24, 6, (1967).

Twomey, S., "Aerosol Size Distribution by Multiple Filter Measurements," J. Atmos. Sci., p. 1073-1079, 33, (1976).

Valley, S.L., "Handbook of Geophysics and Space Environments," Air Force Cambridge Research Laboratories, Chapt. 5, p. 5-1 to 5-27, (1965).

Varley, D.J., Lt. Col., USAF, "Microphysical Properties of a Large Scale Cloud System, 1 - 3 March 1978," AFGL-TR-80-0002, Environmental Research Papers No. 690, Air Force Geophysics Laboratory, (1980).

Wang, P.K., and Pruppacher, H.R., "Acceleration to Terminal Velocity of Cloud and Raindrops," J. Appl. Meteor., p. 275-280, 16, (1977).

Warner, J., and Twomey, S., "The Production of Cloud Nuclei by Cane Fires and the Effect on Cloud Droplet Concentration," J. Atmos. Sci., 24, 6, (1967).

Warner, J., "The Microstructure of Cumulus Cloud. Part I. General Features of the Droplet Spectrum," J. Atmos. Sci., p. 1049-1059, 26, (1969).

Warner, J., "Notes and Correspondence: On the Spatial Variability of Droplets in Cloud," J. Atmos. Sci., p. 541-545, 36, (1979).

Weibel, G.E., and Dressel, H.O., "Propagation Studies in Millimeter-Wave Link Systems," Proceedings of the IEEE, 55, 4, (1967).

Wexler, R. and Atlas, D., "Moisture Supply and Growth of Stratiform Precipitation," J. Meteor., 15, p. 531-539, (1958).

Yamamoto, G. et al., "Table of Scattering Function of Infrared Radiation for Water Clouds," NOAA Technical Report NESS 57 Cat. No. COM-71-50312. GPO, Washington, DC, (1971).

Young, K.C., "The Evolution Of Drop Spectra Due To Condensation, Coalescence, and Breakup," J. Atmos. Sci., 965-973, 32, (1975).

Zissis, G.J., and Wolfe, W.L., et al., "The Infrared Handbook," Environmental Research Institute of Michigan, (1978).

Squires, P. :

-The Microstructure and Colloidal Stability of Warm Clouds. Pt. I. The Relation Between Structure and Stability.," Tellus 10, (1958).

-The Microstructure and Colloidal Stability of Warm Clouds. Pt.II The Causes of the Variations in Microstructure," Tellus, 10, (1958).

-The Microstructure of Cumuli in Maritime and Continental Air," Tellus, 8, 443, (1956).

-The Spatial Variation of Liquid Water and Droplet Concentration In Cumuli," Tellus, 10, 372, (1958).

U.S. Standard Atmospnere, 1976, p. 44-47, NOAA, NASA, USAF, Washington, DC, 1976. Superintendent of Documents.

"Penetrability of Haze, Fog, Clouds and Precipitation by Radiant Energy over the Spectral Range 0.1 Micron to 10 Centimeters," CNA Naval Warfare Analysis Group, Study 61, (1969).

Aerosol Measurement, 1979, Univ. Presses of Florida. D.A.Lundgren et al.

Inadvertent Climate Modification, Report on the Study of Man's Impact on Climate (SMIC) by M.I.T., 1971, M.I.T. Press.

Gunn, R. and Kinzer, D.D., "The Terminal Velocity of Fall of Water Droplets In Stagnant Air," J. Meteorol. 6, p. 243, (1949).

aufm Kampe, H.J., and Weickmann, H.K., "Physics of Clouds," Meteorological Monographs, 3, p. 182, (1957).

Weikmann, H.K., "Physics of Precipitation," Meteorological Monographs, 3, P. 266, (1957).

DATE
ILME